

# Reconfigurable Intelligent Surfaces Aided mmWave NOMA: Joint Power Allocation, Phase Shifts, and Hybrid Beamforming Optimization

Yue Xiu, Jun Zhao, *Member, IEEE*, Wei Sun, *Student Member, IEEE*,  
Marco Di Renzo, *Fellow, IEEE*, Guan Gui, *Senior Member, IEEE*,  
Zhongpei Zhang, *Member, IEEE*, Ning Wei, *Member, IEEE*

## Abstract

In this paper, an reconfigurable intelligent surfaces (RIS)-aided millimeter wave (mmWave) non-orthogonal multiple access (NOMA) systems is considered. In particular, we consider an RIS-aided mmWave-NOMA downlink system with a hybrid beamforming structure. To maximize the achievable sum-rate under a minimum rate constraint for the users and a minimum transmit power constraint, a joint RIS phase shifts, hybrid beamforming, and power allocation problem is formulated. To solve this non-convex optimization problem, we develop an efficient algorithm, called the joint power allocation, hybrid beamforming , and phase shifts optimization (J-PA-HB-PSO) algorithm. Specifically, first, the non-convex problem is transformed into three subproblems, i.e., power allocation, joint phase shifts

Yue Xiu, Zhongpei Zhang, and Ning Wei are with National Key Laboratory of Science and Technology on Communications, University of Electronic Science and Technology of China, Chengdu 611731, China (E-mail: xiuyue@std.uestc.edu.cn, Zhangzp, wn@uestc.edu.cn). Jun Zhao is with School of Computer Science and Engineering, Nanyang Technological University, Singapore (E-mail: junzhao@ntu.edu.sg). Wei Sun is with School of Computer Science and Engineering, Northeastern University, Shenyang 110819, China (E-mail: weisun@stumail.neu.edu.cn). Marco Di Renzo is with Université Paris-Saclay, CNRS, CentraleSupélec, Laboratoire des Signaux et Systèmes, 91192 Gif-sur-Yvette, France. (E-mail: marco.direnzo@centralesupelec.fr). Guan Gui is with College of Telecommunications and Information Engineering, Nanjing University of Posts and Telecommunications, Nanjing 210003, China (E-mail: guiguan@njupt.edu.cn).

This work was supported in part by the Guangdong province Key Project of science and Technology (2018B010115001). The corresponding author is Ning Wei.

and analog beamforming optimization, and digital beamforming design. Then, we solve the power allocation problem under fixed phase shifts of the RIS and hybrid beamforming. Finally, given the power allocation matrix, an alternating manifold optimization (AMO)-based method and a successive convex approximation (SCA)-based method are utilized to design the phase shifts, analog beamforming, and transmit beamforming, respectively. Numerical results reveal that the proposed J-PA-HB-PSO algorithm outperforms state-of-the-art schemes in terms of sum-rate. Moreover, compared to a conventional mmWave-NOMA system without RIS, the proposed RIS-aided mmWave-NOMA system is capable of improving the achievable sum-rate of the system.

### Index Terms

Reconfigurable intelligent surface, millimeter wave, non-orthogonal multiple access, power allocation, phase shifts optimization, hybrid beamforming.

## I. INTRODUCTION

Millimeter wave (mmWave) communications have been proposed as one of the candidate key technologies for the fifth-generation (5G) wireless systems and beyond [1]–[3]. In this context, massive connectivity is a typical requirement for several applications. In conventional systems, however, the data streams are transmitted, in each resource block, by employing an orthogonal multiple access (OMA) scheme [4]. For mmWave communications with the OMA scheme, the number of the users for each data stream in the same time-frequency-code-space resource block is one. Therefore, the total number of served users is limited, which is no greater than the number of RF chains in each resource block [5]. In [6], L. Dai et al. proposed a mmWave non-orthogonal multiple access (NOMA) communication system in order to overcome this issue. Based on this proposal, the signals are transmitted, in each resource block, by using power domain NOMA. In addition, the users experiencing different channel conditions are served simultaneously by employing superposition coding at the transmitter and successive interference cancellation (SIC) at the receiver [7]. This approach can greatly improve the number of served users.

Although mmWave-NOMA has many advantages in terms of improving the communications performance, some limitations may prevent the potential application of mmWave-NOMA. Compared with conventional low-frequency communications, a key challenge of mmWave-NOMA communications is that the transmit signal usually suffers a severe path loss [8]. Furthermore, the use of highly directive antennas makes mmWave-NOMA communications vulnerable to

blockages. Finally, strong user interference may limit the application of mmWave-NOMA. Recently, reconfigurable intelligent surfaces (RISs) have been proposed as a promising technology to alleviate and possibly counteract these problems [9]–[12]. An RIS is a planar array comprising of a large number of reconfigurable passive elements, which can reflect the incident signal by appropriately tuning its amplitude and phase. Therefore, RISs have the capability of enhancing the received signal power and suppress the co-channel interference of the users, as well as overcoming the path loss and signals' blockage of mmWave communications thus making the transfer of information more reliable. In conventional mmWave-NOMA, in addition, the decoding order is determined by the users' channel power gains. By using RISs, the users' decoding order can be designed in a more flexible manner by reconfiguring the RIS phase shifts, which introduces additional degrees-of-freedom (DoF) for improving the performance of mmWave-NOMA systems.

#### *A. Related Work*

Thanks to the many potential benefits, RISs have been investigated for application to various wireless communication systems. In [13], the joint power control and phase shift optimization problem was studied for application to mobile edge computing in RIS-aided mmWave systems. Also, a distributed optimization algorithm was proposed to solve the joint optimization problem. In [14], an architecture for RIS-aided mmWave massive multiple-input multiple-output (MIMO) systems was designed, and two efficient precoders were proposed by exploiting the sparsity of mmWave channels. The design of hybrid analog-digital precoding and phase shift optimization for RIS-aided mmWave systems was investigated in [15], and an iterative algorithm was proposed to minimize the mean-squared-error (MSE). In [16], the joint transmit beamforming and phase shift optimization problem was studied for multi-RIS-aided mmWave systems. For application to multiple-input single-output (MISO) RIS-aided NOMA systems, the semidefinite relaxation method and the manifold optimization method were used to solve the joint transmit beamforming and phase shift optimization problem [17]. A theoretical performance comparison between RIS-NOMA and RIS-OMA was provided in [18], and a low-complexity algorithm was proposed for achieving near-optimal performance. The resource allocation problem for a multi-channel RIS-aided NOMA system was studied in [19], and an algorithm was proposed to jointly optimize the subcarrier assignment, power allocation, and phase shifts. An RIS-aided uplink NOMA system

was considered in [20], and a near-optimal solution was proposed for jointly optimizing the phase shifts and the transmit power. Furthermore, many other research problems in the context of RIS-aided wireless communications have been recently addressed in the literature, which include information rate maximization in [21]–[24], channel estimation in [25], and robust optimization in [26], [27]

### *B. Motivations and Contributions*

Although these papers studied sum-rate enhancement for NOMA-aided wireless communication systems or RIS-aided mmWave communication systems, none of them addressed the analysis and optimization of RIS-aided mmWave-NOMA systems with a hybrid beamforming structure. Moreover, the optimal power allocation and sum-rate maximization in RIS-aided mmWave-NOMA system are challenging tasks to be tackled [7], [28]. Motivated by these considerations, we investigate an RIS-aided mmWave-NOMA system with a hybrid beamforming structures, and provide the following technical contributions:

- To maximize the sum-rate under a minimum rate constraint for each user and a minimum transmit power constraint, we formulate a joint optimization problem for the transmit power, the phase shifts of the RIS, and the hybrid beamforming. An alternating optimization algorithm is proposed to solve this problem.
- By assuming that the phase shifts and the hybrid beamforming are fixed, we propose an algorithm for solving the power allocation problem. Due to the nonconvexity of the considered problem, we divide it into two subproblems and tackle both of them by applying alternating optimization methods.
- We optimize the phase shifts of the RIS and the hybrid beamforming to suppress the interference while maximizing the sum-rate. In the proposed algorithm, the phase shifts and the analog beamforming are designed by using the alternating manifold optimization (AMO) algorithm and by assuming that the transmit power and the digital beamforming weights are fixed. We utilize the successive convex approximation (SCA)-based algorithm to solve the digital beamforming optimization problem. The convergence of the algorithms is proved.
- After optimizing the power allocation, the phase shifts of the RIS, and the hybrid beamforming, we evaluate the performance of the proposed algorithm for application to RIS-

aided mmWave-NOMA systems. The numerical results reveal that the proposed RIS-aided mmWave-NOMA system yields a better sum-rate than a traditional mmWave-NOMA system that does not use RISs. Moreover, we show that the energy efficiency of the proposed RIS-aided mmWave-NOMA scheme is similar to the energy efficiency of a mmWave-NOMA system based on a hybrid beamforming structure.

**Organization:** The rest of the paper is organized as follows. Section II introduces the system model and problem formulation. Section III reports the proposed power allocation algorithm. In Section IV, the AMO algorithm for phase shifts and hybrid beamforming optimization is introduced. Numerical results are illustrated in Section V in order to evaluate the proposed J-PA-HB-PSO algorithm. Finally, Section VI concludes the paper.

**Notation:** The imaginary unit is denoted by  $j = \sqrt{-1}$ . Matrices and vectors are denoted by boldface capital and lower-case letters, respectively.  $\text{diag}\{x_1, \dots, x_N\}$  denotes a diagonal matrix whose diagonal components are  $x_1, \dots, x_N$ . The real and imaginary parts of a complex number  $x$  are denoted by  $\text{Re}(x)$  and  $\text{Im}(x)$ , respectively.  $\mathbf{x}^*$ ,  $\mathbf{x}^T$ , and  $\mathbf{x}^H$  denote the conjugate, transpose, and conjugate transpose of vector  $\mathbf{x}$ , respectively.  $x_n$  and  $X_{k,n}$  denote the  $n$ th and  $(k, n)$ th elements of vector  $\mathbf{x}$  and matrix  $\mathbf{X}$ , respectively.  $\|\mathbf{x}\|$  denotes the 2-norm of vector  $\mathbf{x}$ .  $\mathcal{CN}(x, \sigma^2)$  denotes the Gaussian distribution, where  $x$  and  $\sigma$  are the mean and variance, respectively.

## II. SYSTEM MODEL AND PROBLEM FORMULATION

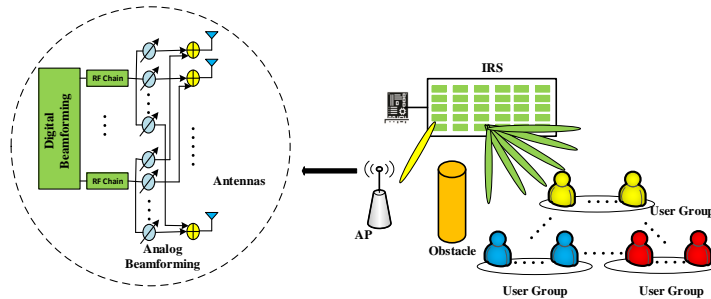


Fig. 1. Illustration of the downlink multi-group multi-user RIS-aided mmWave-NOMA communication system.

As shown in Fig.1, an RIS-aided mmWave-NOMA system is considered. The access point (AP) is equipped with a hybrid beamforming structure, where the number of transmit antennas

and radio frequency (RF) chains are  $N_t$  and  $N_{RF}$ , respectively.  $K$  users equipped with a single antenna are distributed in  $N$  groups, with  $K > N_{RF}$ . Let  $\mathbf{s} \in \mathbb{C}^{K \times 1}$  be the transmitted signals, where  $\mathbb{E}(\mathbf{s}\mathbf{s}^H) = \mathbf{I}$ . The data streams are precoded by the digital beamforming matrix  $\mathbf{W} \in \mathbb{C}^{N_{RF} \times N_s}$ , where  $N_s$  is the length of each data stream. Then, an analog beamforming matrix  $\mathbf{F} \in \mathbb{C}^{N_t \times N_{RF}}$  is applied. Analog beamforming is realized by using  $N_t$  phase shifters. The number of data streams is assumed to be equal to the number of RF chains. In particular, each independent data stream corresponds to a group, i.e.,  $N = N_s = N_{RF}$ . The signals transmitted by the AP reach the RIS through the wireless channel. The RIS applies a phase shift matrix  $\mathbf{\Theta} = \text{diag}(\boldsymbol{\theta}) \in \mathbb{C}^{N_r \times N_r}$  to the incident signals, where  $\boldsymbol{\theta} = [e^{j\theta_1}, \dots, e^{j\theta_{N_r}}]^T \in \mathbb{C}^{N_r \times 1}$ ,  $0 \leq \theta_i \leq 2\pi$ ,  $1 \leq i \leq N_r$  and  $N_r$  is the number of reflecting elements of the RIS. The users perform successive interference cancellation (SIC) on the signals reflected by the RIS. In particular, SIC is applied to users in the same group. We denote by  $\mathcal{G}_n$  the  $n$ th group, which fulfills the properties  $\mathcal{G}_i \cap \mathcal{G}_j = \emptyset$ ,  $\forall i \neq j$ , where  $\emptyset$  denotes the empty set,  $\sum_{n=1}^N |\mathcal{G}_n| = K$ , and  $|\mathcal{G}_n|$  is the number of users in  $\mathcal{G}_n$ . In our system model, we assume that the direct link between the AP and the user is blocked, which is a typical application scenario when RISs are needed or used [29]. The AP-to-RIS channel is denoted by  $\mathbf{G} \in \mathbb{C}^{N_r \times N_t}$ , and the channel between the RIS and the user  $k$  in the  $n$ th group is denoted by  $\mathbf{h}_{n,k} \in \mathbb{C}^{N_r \times 1}$ . Then, the received signal for the  $k$ th user in the  $n$ th group can be written as follows

$$y_{n,k} = \mathbf{h}_{n,k}^H \mathbf{\Theta} \mathbf{G} \mathbf{F} \mathbf{W} \mathbf{P} \mathbf{s} + u_{n,k}, \quad (1)$$

where  $u_{n,k} \sim \mathcal{CN}(0, \sigma^2)$  is the noise at the user, and  $\mathbf{P} = \text{diag}\{\mathbf{p}_1, \mathbf{p}_2, \dots, \mathbf{p}_N\} \in \mathbb{C}^{N \times K}$  is the power allocation matrix, where  $\mathbf{p}_n = [\sqrt{p_{n,1}}, \dots, \sqrt{p_{n,|\mathcal{G}_n|}}] \in \mathbb{C}^{1 \times |\mathcal{G}_n|}$ . The analog beamforming matrix  $\mathbf{F}$  and phase shift vector  $\boldsymbol{\theta}$  with constant modulus constraint are defined as follows [9]

$$|\mathbf{F}_{i,j}| = \frac{1}{\sqrt{N_t}}, \quad 1 \leq i \leq N_t, 1 \leq j \leq N_{RF}, |\boldsymbol{\theta}_i| = 1, \quad 1 \leq i \leq N_r. \quad (2)$$

The hybrid beamforming matrix is defined as

$$\mathbf{D} = \mathbf{F} \mathbf{W} = [\mathbf{d}_1, \mathbf{d}_2, \dots, \mathbf{d}_N]. \quad (3)$$

Since the transmission power is separated from the hybrid beamforming matrix, each column of

$D$  fulfills the property

$$\|\mathbf{d}_n\| = 1, \quad 1 \leq n \leq N. \quad (4)$$

Measurement campaigns showed that the power of the mmWave line-of-sight (LoS) path is usually much higher (about 13 dB higher) than the sum of the powers of non-line-of-sight (NLoS) paths [30]. Considering this fact, it is desirable to make sure that the channel between the AP and the RIS is in LoS. In practice, by assuming that the location of the AP is known, the location of the RIS can be appropriately chosen so as to ensure that the AP-RIS channel is in LoS. Based on these considerations, we assume that the channel from the AP to the RIS is or can be well approximated by a rank-one matrix, i.e.,

$$\mathbf{G} = \alpha \mathbf{a}_r(\phi) \mathbf{a}_t^T(\vartheta), \quad (5)$$

where  $\alpha$  is a scaling factor accounting for the antenna and path gains, where  $\mathbf{a}_t(\vartheta) \in \mathbb{C}^{N_t \times 1}$  and  $\mathbf{a}_r(\phi) \in \mathbb{C}^{N_r \times 1}$  represent the normalized array response vectors associated with the AP and the RIS, respectively. The channel from the RIS to the  $k$ th user in the  $n$ th group is generated according to the following geometric channel model [31]

$$\mathbf{h}_{n,k} = \sum_{l=0}^{L_{n,k}-1} \beta_{n,k}^l \mathbf{b}_t(\theta_l), \quad (6)$$

where  $\beta_{n,k}^l$  is a scaling factor accounting for the antenna and path gains,  $\mathbf{b}_t(\theta_l) \in \mathbb{C}^{N_r \times 1}$  represents the normalized array response vector of the RIS, and  $L_{n,k}$  is the total number of paths.

In power domain NOMA, in general, the optimal decoding order of the users is determined based on the users' channel gains [32]. In an RIS-aided mmWave-NOMA system with hybrid beamforming, on the other hand, the decoding order is determined by the channel gains and by the beamforming gains. Therefore, it is necessary to first determine the decoding order. Without loss of generality, we assume the decoding order in the  $n$ th group is  $|\mathbf{h}_{n,1}^H \mathbf{\Theta} \mathbf{G} \mathbf{F} \mathbf{w}_n|^2 \geq |\mathbf{h}_{n,2}^H \mathbf{\Theta} \mathbf{G} \mathbf{F} \mathbf{w}_n|^2 \geq \dots \geq |\mathbf{h}_{n,|\mathcal{G}_n|}^H \mathbf{\Theta} \mathbf{G} \mathbf{F} \mathbf{w}_n|^2$ , which implies that the optimal decoding order is determined by the effective channel gains, ranked in increasing order of magnitude [4], [5], [33]. Thus, the user  $k$  in the group  $n$  can decode  $s_{n,k}$  ( $n+1 \leq j \leq |\mathcal{G}_n|$ ), which is then removed from the received signal. The other signals are treated as interference. Therefore, the signal to

interference plus noise ratio (SINR) of the user  $k$  in group  $n$  is given by

$$\text{SINR}_{n,k} = \frac{|\mathbf{h}_{n,k}^H \mathbf{\Theta} \mathbf{G} \mathbf{F} \mathbf{w}_n|^2 p_{n,k}}{|\mathbf{h}_{n,k}^H \mathbf{\Theta} \mathbf{G} \mathbf{F} \mathbf{w}_n|^2 \sum_{j=1}^{k-1} p_{n,j} + \sum_{i \neq n} \sum_{j=1}^{|\mathcal{G}_i|} |\mathbf{h}_{n,k}^H \mathbf{\Theta} \mathbf{G} \mathbf{F} \mathbf{w}_i|^2 p_{i,j} + \sigma^2}. \quad (7)$$

In addition, we assume that the interference from other groups can be well suppressed if the following holds

$$|\mathbf{h}_{n,k}^H \mathbf{\Theta} \mathbf{G} \mathbf{F} \mathbf{w}_i|^2 \leq \tau, \quad i \neq n, \quad (8)$$

where  $\tau$  is small enough. Therefore, the main interference originates from other users in the same group. Under these assumptions the  $\text{SINR}_{n,k}$  can be approximated as

$$\text{SINR}_{n,k} \approx \frac{|\mathbf{h}_{n,k}^H \mathbf{\Theta} \mathbf{G} \mathbf{F} \mathbf{w}_n|^2 p_{n,k}}{|\mathbf{h}_{n,k}^H \mathbf{\Theta} \mathbf{G} \mathbf{F} \mathbf{w}_n|^2 \sum_{j=1}^{k-1} p_{n,j} + \sigma^2}. \quad (9)$$

According to (9), the achievable rate of the user  $k$  in group  $n$  can be written as

$$R_{n,k} = \log_2(1 + \text{SINR}_{n,k}). \quad (10)$$

Finally, the sum-rate of the RIS-aided mmWave-NOMA system can be written as

$$R = \sum_{n=1}^N \sum_{k=1}^{|\mathcal{G}_n|} R_{n,k}. \quad (11)$$

We assume that the AP-to-RIS channel and RIS-to-user channel are known by the AP, and that all optimization operations are executed at the AP. Based on (9)-(11), the sum-rate optimization problem for RIS-aided mmWave-NOMA with hybrid beamforming can be formulated as

$$\max_{\mathbf{w}, \mathbf{\Theta}, \mathbf{F}, \{p_{n,k}\}} R \quad (12a)$$

$$\text{s.t. } R_{n,k} \geq \gamma_{n,k} \quad (12b)$$

$$p_{n,k} \geq 0, \quad (12c)$$

$$\sum_{n=1}^N \sum_{k=1}^{|\mathcal{G}_n|} p_{n,k} \leq P, \quad (12d)$$

$$|\mathbf{F}_{i,j}| = \frac{1}{\sqrt{N}}, 1 \leq i \leq N_t, 1 \leq j \leq N_{RF}, \quad (12e)$$

$$|\mathbf{\theta}_i| = 1, 1 \leq i \leq N_r, \quad (12f)$$



$$\mathbf{D} = \mathbf{F}\mathbf{W}, \quad (12g)$$

$$\|\mathbf{d}_n\| = 1, 1 \leq n \leq N, \quad (12h)$$

$$|\mathbf{h}_{n,k}^H \boldsymbol{\Theta} \mathbf{G} \mathbf{F} \mathbf{w}_i|^2 \leq \tau, \quad i \neq n. \quad (12i)$$

The size of all variables in the problem (12) is  $N_{RF}N_s + N_{RF}N_t + K + N_r$ , which is usually large. Two major challenges render the solution of the optimization problem in (12) difficult to tackle. The first difficulty is that the optimized variables are coupled, which makes the problem non-convex. The second difficulty is the decoding order. Usually, the optimal decoding order corresponds to the increasing order of the users' effective channel gains. However, the ordering of the effective channel gains varies with the beamforming matrix and the phase shift matrix. These challenges make the problem in (12) difficult to solve. To tackle both issues, a J-PA-HB-PSO algorithm is proposed, which includes three parts, i.e., power optimization, analog beamforming and RIS phase shifts optimization, and transmit beamforming optimization. These three sub-parts are analyzed in the following sections.

### III. POWER ALLOCATION OPTIMIZATION

For a given hybrid beamforming matrix and a given phase shifts matrix of the RIS, (12) can be simplified as

$$\max_{\{p_{n,k}\}} R \quad (13a)$$

$$\text{s.t. (12b), (12c), (12d).} \quad (13b)$$

When the hybrid beamforming matrix and the phase shifts matrix of the RIS are fixed, the decoding order is fixed. This simplifies the optimization problem to solve. Without loss of generality, we assume  $|\mathbf{h}_{n,1}^H \boldsymbol{\Theta} \mathbf{G} \mathbf{F} \mathbf{w}_n|^2 \geq |\mathbf{h}_{n,2}^H \boldsymbol{\Theta} \mathbf{G} \mathbf{F} \mathbf{w}_n|^2 \geq \dots \geq |\mathbf{h}_{n,|\mathcal{G}_n|}^H \boldsymbol{\Theta} \mathbf{G} \mathbf{F} \mathbf{w}_n|^2$ . Although the decoding order is fixed, the objective function and the constraint (12b) in (12) are still non-convex. To address this issue, we introduce the auxiliary variables  $\{P_n\}$  and  $P_n = \sum_{k=1}^{|\mathcal{G}_n|} p_{n,k}$ ,  $\forall i \leq n \leq N$ , which denotes the power allocated to the  $n$ th group. Therefore, (13) is reformulated as

$$\max_{\{P_n\}} \max_{\{p_{n,k}\}} R \quad (14a)$$

$$\text{s.t. (12b), (12c),} \quad (14b)$$

$$\sum_{k=1}^{|\mathcal{G}_n|} p_{n,k} = P_n, \quad (14c)$$

$$\sum_{n=1}^N P_n = P. \quad (14d)$$

Since we assume that the interference from other groups can be suppressed, according to (9), a user in group  $n$  is mainly interfered by other users in group  $n$ . Based on the considered decoding order and taking into account the results in the results in [34], the maximization of the sum-rate corresponds to setting,  $R_{n,k} = \gamma_k$ ,  $\forall 1 \leq n \leq N$ ,  $2 \leq k \leq |\mathcal{G}_n|$ , i.e., the user with the higher decoding order are allocated as much power as possible if the other users meet the minimum rate requirements. Hence, the solution of the power allocation problem in group  $n$  corresponds to the following equations

$$R_{n,2} = \gamma_{n,2}, \dots, R_{n,|\mathcal{G}_n|} = \gamma_{n,|\mathcal{G}_n|}, \sum_{k=1}^{|\mathcal{G}_n|} p_{n,k} = P_n. \quad (15)$$

From (11) and (12), the solution of equation (15) is

$$\begin{aligned} p_{n,|\mathcal{G}_n|} &= \frac{2^{\gamma_{n,|\mathcal{G}_n|}}}{1 + 2^{\gamma_{n,|\mathcal{G}_n|}}} \left( P_n + \frac{\sigma^2}{|\mathbf{h}_{n,|\mathcal{G}_n|} \mathbf{\Theta} \mathbf{G} \mathbf{F} \mathbf{w}_n|^2} \right), \\ &\vdots \\ p_{n,2} &= \frac{2^{\gamma_{n,2}}}{1 + 2^{\gamma_{n,2}}} \left( P_n - \sum_{k=3}^{|\mathcal{G}_n|} p_{n,k} + \frac{\sigma^2}{|\mathbf{h}_{n,2} \mathbf{\Theta} \mathbf{G} \mathbf{F} \mathbf{w}_n|^2} \right), \\ p_{n,1} &= P_n - \sum_{k=2}^{|\mathcal{G}_n|} p_{n,k}. \end{aligned} \quad (16)$$

Since  $R_{n,2} = \gamma_{n,2}, \dots, R_{n,|\mathcal{G}_n|} = \gamma_{n,|\mathcal{G}_n|}$ , the objective function in (14a) can be rewritten as

$$R = \sum_{n=1}^N R_{n,1} + \sum_{n=1}^N \sum_{k=2}^{|\mathcal{G}_n|} \gamma_{n,k}. \quad (17)$$

Since  $\sum_{n=1}^N \sum_{k=2}^{|\mathcal{G}_n|} \gamma_{n,k}$  is a constant, (14) is further simplified as

$$\max_{\{P_n\}} \sum_{n=1}^N R_{n,1}, \quad (18a)$$

$$\text{s.t. (12b), (14d).} \quad (18b)$$

Because the objective function (18a) is non-convex, solving problem (18) is still difficult. We propose an iterative algorithm to tackle it. To this end, we note that the optimization problem in (18) without (12d) is convex. Hence, we have the following **Theorem 1**.

**Theorem 1.** *When the constraint (12b) is removed, the globally optimal solution of (18) is*

$$\bar{P}_n = \frac{P}{N} - \frac{\alpha_n + 1}{\beta_n} + \sum_{i=1}^N \frac{\alpha_i + 1}{N\beta_i}, \quad (19)$$

where

$$\beta_n = \frac{|\mathbf{h}_{n,1}^H \mathbf{\Theta G F w}_n|^2}{\sigma^2} \left( 1 - \sum_{k=2}^{|\mathcal{G}_n|} \left[ (2^{\gamma_{n,k}} - 1) \prod_{j=2}^k \frac{1}{2^{\gamma_{n,j}}} \right] \right) \quad (20)$$

and

$$\alpha_n = - \frac{|\mathbf{h}_{n,1}^H \mathbf{\Theta G F w}_n|^2}{\sigma^2} \sum_{k=2}^{|\mathcal{G}_n|} \left[ (2^{\gamma_{n,k}} - 1) \frac{\sigma^2}{|\mathbf{h}_{n,k}^H \mathbf{\Theta G F w}_k|^2} \prod_{j=2}^k \frac{1}{2^{\gamma_{n,j}}} \right]. \quad (21)$$

The proof is given in **Appendix A**.

Based on **Theorem 1**, if  $\bar{P}_n$  in (19) satisfies the constraint in (12b), i.e.,  $\frac{|\mathbf{h}_{n,k}^H \mathbf{\Theta G F w}_n|^2 p_{n,k}}{|\mathbf{h}_{n,k}^H \mathbf{\Theta G F w}_n|^2 (\bar{P}_n - p_{n,k}) + \sigma^2} \geq 2^{\gamma_{n,k}} - 1$ ,  $\bar{P}_n$  is the optimal solution of (18). However, if  $\bar{P}_n$  do not satisfy the constraint in (12b), i.e.,  $\frac{|\mathbf{h}_{n,k}^H \mathbf{\Theta G F w}_n|^2 p_{n,k}}{|\mathbf{h}_{n,k}^H \mathbf{\Theta G F w}_n|^2 (\bar{P}_n - p_{n,k}) + \sigma^2} \leq 2^{\gamma_{n,k}} - 1$ ,  $\bar{P}_n$  is not the optimal solution of (18). In this latter case, the result in **Theorem 2** can be used.

**Theorem 2.** *When the constraint (12b) is considered, the globally optimal solution should always satisfy*

$$\hat{P}_n = \frac{2^{\gamma_{n,1}} - \alpha_n}{\beta_n}, \quad \forall n \in \left\{ n | 1 \leq n \leq N, \frac{|\mathbf{h}_{n,k}^H \mathbf{\Theta G F w}_n|^2 p_{n,k}}{|\mathbf{h}_{n,k}^H \mathbf{\Theta G F w}_n|^2 (\bar{P}_n - p_{n,k}) + \sigma^2} < 2^{\gamma_{n,k}} - 1 \right\}. \quad (22)$$

The proof is given in **Appendix B**.

When  $n \in \left\{ n | 1 \leq n \leq N, \frac{|\mathbf{h}_{n,k}^H \mathbf{\Theta G F w}_n|^2 p_{n,k}}{|\mathbf{h}_{n,k}^H \mathbf{\Theta G F w}_n|^2 (\bar{P}_n - p_{n,k}) + \sigma^2} \leq 2^{\gamma_{n,k}} - 1 \right\}$ , the optimal power allocation can be obtained by solving the following problem

$$\max_{\{P_n\}} \sum_{n \notin \mathcal{N}} R_{n,1} \quad (23a)$$

$$\text{s.t. } R_{n,1} \geq r_{n,1}, \quad (23b)$$

$$\sum_{n \notin \mathcal{N}} P_n \leq P - \sum_{j \in \mathcal{N}} \hat{P}_j, \quad (23c)$$

where  $\mathcal{N} = \left\{ n \mid 1 \leq n \leq N, \frac{|\mathbf{h}_{n,k}^H \boldsymbol{\Theta} \mathbf{G} \mathbf{F} \mathbf{w}_n|^2 p_{n,k}}{|\mathbf{h}_{n,k}^H \boldsymbol{\Theta} \mathbf{G} \mathbf{F} \mathbf{w}_n|^2 (\bar{P}_n - p_{n,k}) + \sigma^2} \leq 2^{\gamma_{n,k}} - 1 \right\}$ . Based on (23), the proposed algorithms consists of the following steps. First, we consider the problem in (23) by ignoring the constraint (23b). In this case, **Theorem 1** can be used. Then, we use **Theorem 2** in order to obtain the solutions that do not satisfy the constraint (23b), and update problem (23). This procedure is iterated until convergence, as reported in **Algorithm 1**.

---

**Algorithm 1:** Proposed Group Power Allocation Algorithm

---

- 1 **Initialization:**  $t = 0$ ,  $P_n^{(t)} = P_n^{(0)} = \frac{P}{N_{RF}}$ .
  - 2 **Repeat:**
  - 3  $\mathcal{V} = \{1, 2, \dots, N\}$ , let  $\mathcal{N} = \mathcal{V}$ .
  - 4 **If:**  $\mathcal{N} \neq \emptyset$
  - 5 **Repeat:**
  - 6 According to **Theorem 1**, calculate  $\beta_n$ ,  $\alpha_n$ , and  $\bar{P}_n^{(t)}$ .
  - 7 Update  $\mathcal{N} = \left\{ n \mid 1 \leq n \leq N, \frac{|\mathbf{h}_{n,k}^H \boldsymbol{\Theta} \mathbf{G} \mathbf{F} \mathbf{w}_n|^2 p_{n,k}}{|\mathbf{h}_{n,k}^H \boldsymbol{\Theta} \mathbf{G} \mathbf{F} \mathbf{w}_n|^2 (\bar{P}_n - p_{n,k}) + \sigma^2} \leq 2^{\gamma_{n,k}} - 1 \right\}$ .
  - 8 According to **Theorem 2**, calculate  $\hat{P}_n^{(t)}$ .
  - 9 Update the set according to  $\mathcal{V} = \mathcal{V} / \mathcal{N}$ .
  - 10 **Until:**  $\mathcal{N} = \emptyset$ .
  - 11 **Update:**  $\hat{P}_n^{(t)} = \bar{P}_n^{(t)}$ .
  - 12 **Until:**  $P_n^* = \hat{P}_n^{(T_{max})}$ , where  $T_{max}$  is maximize the number of iterations.
  - 13 **Output:**  $\{P_n^*\}$ .
- 

#### IV. PHASE SHIFTS AND HYBRID BEAMFORMING DESIGN

Given  $\{p_{n,k}\}$  and  $\{P_n\}$ , the original problem in (12) can be simplified as follows

$$\max_{\boldsymbol{\Theta}, \mathbf{F}, \mathbf{W}} R \quad (24a)$$

$$\text{s.t. (12b), (12e), (12f), (12g), (12h), (12i).} \quad (24b)$$

The non-convex modulus constraints for the analog beamforming and the phase shifts of the RIS make the solving (24a) difficult. To tackle (24a), we propose a suboptimal algorithm. First, we introduce the auxiliary variables  $\{\mathbf{u}_i\}$ ,  $\{v_{n,k,i}\}$ ,  $\{z_{n,k,i}\}$ , such that

$$\mathbf{u}_i = \mathbf{G}\mathbf{F}\mathbf{w}_i, v_{n,k,i} = \mathbf{h}_{n,k}^H \Theta \mathbf{u}_i, z_{n,k,i} = v_{n,k,i} v_{n,k,i}^H. \quad (25)$$

Substituting (25) into (12a), the problem in (12) can be rewritten as

$$\max_{\mathbf{W}, \Theta, \mathbf{F}, \{\mathbf{u}_i\}, \{v_{n,k,i}\}, \{z_{n,k,i}\}} \sum_{n=1}^N \sum_{k=1}^{|\mathcal{G}_n|} \log_2 \left( 1 + \frac{z_{n,k,n} p_{n,k}}{z_{n,k,n} \sum_{j=1}^{k-1} p_{n,j} + \sigma^2} \right) \quad (26a)$$

$$\text{s.t. } z_{n,k,n} p_{n,k} - (2^{\gamma_{n,k}} - 1) \left( z_{n,k,n} \sum_{j=1}^{k-1} p_{n,j} + \sigma^2 \right) \leq 0 \quad (26b)$$

$$(12e), (12f), (12g), (12h), \quad (26c)$$

$$\mathbf{u}_i = \mathbf{G}\mathbf{F}\mathbf{w}_i, \quad (26d)$$

$$v_{n,k,i} = \mathbf{h}_{n,k}^H \Theta \mathbf{u}_i, \quad (26e)$$

$$z_{n,k,i} = v_{n,k,i} v_{n,k,i}^H, \quad (26f)$$

$$z_{n,k,i} \leq \tau, i \neq n. \quad (26g)$$

In order to transform the objective function in (26a) into a difference of convex (DC) programming problem, we note that the objective function (26a) is equal to

$$\sum_{n=1}^N \sum_{k=1}^{|\mathcal{G}_n|} \log_2 \left( z_{n,k,n} \sum_{j=1}^k p_{n,j} + \sigma^2 \right) - \sum_{n=1}^N \sum_{k=1}^{|\mathcal{G}_n|} \log_2 \left( z_{n,k,n} \sum_{j=1}^{k-1} p_{n,j} + \sigma^2 \right). \quad (27)$$

According to [35], the problem in (26) is equivalent to

$$\min_{\mathbf{W}, \Theta, \mathbf{F}, \{\mathbf{u}_i\}, \{v_{n,k,i}\}, \{z_{n,k,i}\}} \sum_{n=1}^N \sum_{k=1}^{|\mathcal{G}_n|} \log_2 \left( z_{n,k,n} \sum_{j=1}^{k-1} p_{n,j} + \sigma^2 \right) - \sum_{n=1}^N \sum_{k=1}^{|\mathcal{G}_n|} \log_2 \left( z_{n,k,n} \sum_{j=1}^k p_{n,j} + \sigma^2 \right) \quad (28a)$$

$$\text{s.t. } (12e), (12f), (12g), (12h), (26b),$$

$$(26d), (26e), (26f), (26g). \quad (28b)$$

Now, we focus on the constraint (26f). The following theorem holds.

**Theorem 3.** *Constraint (26f) is equivalent to the following*

$$\begin{bmatrix} z_{n,k,i} & v_{n,k,i} \\ v_{n,k,i}^H & 1 \end{bmatrix} \succeq \mathbf{0}, \quad (29)$$

and

$$z_{n,k,i} - v_{n,k,i} v_{n,k,i}^H \leq 0. \quad (30)$$

The proof is given in **Appendix C**.

Substituting (29) and (30) into (28), the problem in (28) is rewritten as

$$\min_{\mathbf{W}, \Theta, \mathbf{F}, \{\mathbf{u}_i\}, \{v_{n,k,i}\}, \{z_{n,k,i}\}} \sum_{n=1}^N \sum_{k=1}^{|\mathcal{G}_n|} \log_2(z_{n,k,n} \sum_{j=1}^{k-1} p_{n,j} + \sigma^2) - \sum_{n=1}^N \sum_{k=1}^{|\mathcal{G}_n|} \log_2(z_{n,k,n} \sum_{j=1}^k p_{n,j} + \sigma^2) \quad (31a)$$

$$\text{s.t. (12e), (12f), (12g), (12h), (26b),}$$

$$(26d), (26e), (26g) \quad (31b)$$

$$(z_{n,k,i} - v_{n,k,i} v_{n,k,i}^H) \leq 0, \quad (31c)$$

$$\begin{bmatrix} z_{n,k,i} & v_{n,k,i} \\ v_{n,k,i}^H & 1 \end{bmatrix} \succeq \mathbf{0}. \quad (31d)$$

Employing the exact penalty method [35], (31) can be rewritten as

$$\begin{aligned} \min_{\mathbf{W}, \Theta, \mathbf{F}, \{\mathbf{u}_i\}, \{v_{n,k,i}\}, \{z_{n,k,i}\}} & \sum_{n=1}^N \sum_{k=1}^{|\mathcal{G}_n|} \log_2(z_{n,k,n} \sum_{j=1}^{k-1} p_{n,j} + \sigma^2) - \sum_{n=1}^N \sum_{k=1}^{|\mathcal{G}_n|} \log_2(z_{n,k,n} \sum_{j=1}^k p_{n,j} + \sigma^2) \\ & + \lambda \left( \sum_{i=1}^N \|\mathbf{u}_i - \mathbf{G}\mathbf{F}\mathbf{w}_i\|^2 + \|\mathbf{D} - \mathbf{F}\mathbf{W}\|^2 + \sum_{n=1}^N \sum_{k=1}^{|\mathcal{G}_n|} \sum_{i=1}^N \|v_{n,k,i} - \mathbf{h}_{n,k}^H \Theta \mathbf{u}_i\|^2 + \sum_{n=1}^N \right. \\ & \left. \sum_{k=1}^{|\mathcal{G}_n|} \sum_{i=1}^N (z_{n,k,i} - v_{n,k,i} v_{n,k,i}^H) \right) \end{aligned} \quad (32a)$$

$$\text{s.t. (12e), (12f), (12g), (12h), (26b),}$$

$$(26g), (31c), (31d). \quad (32b)$$

We observe that the minuend and the subtrahend in the objective function and the constraints (26b), (26g), and (31d) are convex, but the constraints (12e)-(12h) and (31c) are still non-

convex. To deal with the non-convex constraints in (12e), (12f), and (12h), we propose an AMO algorithm.

#### A. Phase Shift and Analog Beamforming Design Based on the AMO Algorithm

For a fixed transmit beamforming and power allocation matrix, problem (32) simplifies to

$$\begin{aligned} \min_{\mathbf{D}, \mathbf{\Theta}, \mathbf{F}} & \sum_{n=1}^N \sum_{k=1}^{|\mathcal{G}_n|} \log_2(z_{n,k,n} \sum_{j=1}^{k-1} p_{n,j} + \sigma^2) - \sum_{n=1}^N \sum_{k=1}^{|\mathcal{G}_n|} \log_2(z_{n,k,n} \sum_{j=1}^k p_{n,j} + \sigma^2) \\ & + \lambda \left( \sum_{i=1}^N \|\mathbf{u}_i - \mathbf{G}\mathbf{F}\mathbf{w}_i\|^2 + \|\mathbf{D} - \mathbf{F}\mathbf{W}\|^2 + \sum_{n=1}^N \sum_{k=1}^{|\mathcal{G}_n|} \sum_{i=1}^N \|v_{n,k,i} - \mathbf{h}_{n,k}^H \mathbf{\Theta} \mathbf{u}_i\|^2 \right. \\ & \left. + \sum_{n=1}^N \sum_{k=1}^{|\mathcal{G}_n|} \sum_{i=1}^N (z_{n,k,i} - v_{n,k,i} v_{n,k,i}^H) \right) \end{aligned} \quad (33a)$$

$$\text{s.t. (12e), (12f), (12h),} \quad (33b)$$

According to the notion of manifold optimization, problem (33) can be reformulated in three sub-problems:

$$\min_{\mathcal{M}_1} \sum_{n=1}^N \sum_{k=1}^{|\mathcal{G}_n|} \sum_{i=1}^N \|v_{n,k,i} - \mathbf{h}_{n,k}^H \mathbf{\Theta} \mathbf{u}_i\|^2, \quad (34)$$

$$\min_{\mathcal{M}_2} \sum_{i=1}^N \|\mathbf{u}_i - \mathbf{G}\mathbf{F}\mathbf{w}_i\|^2 + \|\mathbf{D} - \mathbf{F}\mathbf{W}\|^2, \quad (35)$$

$$\min_{\mathcal{M}_3} \|\mathbf{D} - \mathbf{F}\mathbf{W}\|^2, \quad (36)$$

where  $\mathcal{M}_1$ ,  $\mathcal{M}_2$ , and  $\mathcal{M}_3$  are the manifold space defined in the constant modulus constraints in (12e)-(12f). Then,  $\mathcal{M}_1$ ,  $\mathcal{M}_2$ , and  $\mathcal{M}_3$  are expressed as

$$\mathcal{M}_1 = \{\mathbf{\Theta} \in \mathbb{C}^{N_r \times 1} | |\theta_1| = \dots = |\theta_{N_r}| = 1\}, \quad (37)$$

$$\mathcal{M}_2 = \{\mathbf{F} \in \mathbb{C}^{N_t \times N_{RF}} | |F_{1,1}| = \dots = |F_{N_t, N_{RF}}| = 1\}, \quad (38)$$

$$\mathcal{M}_3 = \{\mathbf{D} \in \mathbb{C}^{N_t \times N} | \mathbf{D}\mathbf{D}^H \odot \mathbf{I} = \mathbf{I}\}, \quad (39)$$

In particular,  $\mathcal{M}_1$  and  $\mathcal{M}_2$  are called Riemannian manifolds, and  $\mathcal{M}_3$  is called Oblique manifold [36]. The principle of manifold optimization method is to apply the gradient descent algorithm in the manifold space. In particular, the gradient descent algorithm on Riemannian manifolds

is similar to that in Euclidean spaces. However, the Riemannian gradient is used for the search direction. The Riemannian gradients of (34)-(36) at the current point  $\boldsymbol{\theta}$ ,  $\mathbf{F}$ ,  $\mathbf{D}$  are defined as the projection of the search direction in the Euclidean space onto the tangent spaces  $\mathcal{T}_{\boldsymbol{\theta}}\mathcal{M}_1$ ,  $\mathcal{T}_{\mathbf{F}}\mathcal{M}_2$ , and  $\mathcal{T}_{\mathbf{D}}\mathcal{M}_3$ , which can be expressed as

$$\mathcal{T}_{\boldsymbol{\theta}}\mathcal{M}_1 = \{\mathbf{u} \in \mathbb{C}^{N_r \times 1} | \text{Re}\{\boldsymbol{\theta}^H \odot \mathbf{u}\} = 0\}, \quad (40)$$

$$\mathcal{T}_{\mathbf{F}}\mathcal{M}_2 = \{\mathbf{U} \in \mathbb{C}^{N \times N_{RF}} | \text{Re}\{\mathbf{F}^H \odot \mathbf{U}\} = 0\}, \quad (41)$$

$$\mathcal{T}_{\mathbf{D}}\mathcal{M}_3 = \{\mathbf{V} \in \mathbb{C}^{N_r \times N_{RF}} | \text{Re}\{\mathbf{I} \odot \text{Re}(\mathbf{D}\mathbf{V}^H)\} = 0\}. \quad (42)$$

where  $\odot$  denotes the Hadamard product. Then, the Euclidean gradients of (34)-(36) at  $\boldsymbol{\theta}$ ,  $\mathbf{F}$ , and  $\mathbf{D}$  are computed as follows

$$\nabla_{\boldsymbol{\theta}} f_1(\boldsymbol{\theta}) = \sum_{n=1}^N \sum_{k=1}^{|\mathcal{G}_n|} \sum_{i=1}^N \text{diag}(\mathbf{h}_{n,k}^H) \mathbf{u}_i \mathbf{u}_i^H \text{diag}(\mathbf{h}_{n,k}) \boldsymbol{\theta}^* - \mathbf{h}_{n,k}^* \odot \mathbf{u}_i \mathbf{u}_{n,k,i}^*, \quad (43)$$

$$\nabla_{\mathbf{F}} f_2(\mathbf{F}) = \sum_{i=1}^N \mathbf{G}^T \mathbf{G}^* \mathbf{F}^* \mathbf{w}_i^* \mathbf{w}_i^T - \sum_{i=1}^N \mathbf{G}^T \mathbf{u}_i^* \mathbf{w}_i^T + \mathbf{F}^* \mathbf{W}^* \mathbf{W}^T - \mathbf{D}^* \mathbf{W}^T, \quad (44)$$

$$\nabla_{\mathbf{D}} f_3(\mathbf{D}) = \mathbf{D}^* - \mathbf{F}^* \mathbf{W}^*, \quad (45)$$

where  $f_1(\boldsymbol{\theta}) = \sum_{n=1}^N \sum_{k=1}^{|\mathcal{G}_n|} \sum_{i=1}^N \|v_{n,k,i} - \mathbf{h}_{n,k}^H \boldsymbol{\theta} \mathbf{u}_i\|$ ,  $f_2(\mathbf{F}) = \sum_{i=1}^N \|\mathbf{u}_i - \mathbf{G} \mathbf{F} \mathbf{w}_i\| + \|\mathbf{D} - \mathbf{F} \mathbf{W}\|$ ,  $f_3(\mathbf{D}) = \|\mathbf{D} - \mathbf{F} \mathbf{W}\|$ . Based on the Euclidean gradient, the Riemannian gradients of (34)-(36) are expressed as

$$\text{grad}_{\boldsymbol{\theta}} f_1(\boldsymbol{\theta}) = \nabla_{\boldsymbol{\theta}} f_1(\boldsymbol{\theta}) - \text{Re}\{\nabla_{\boldsymbol{\theta}} f_1(\boldsymbol{\theta}) \odot \boldsymbol{\theta}\} \odot \boldsymbol{\theta}, \quad (46)$$

$$\text{grad}_{\mathbf{F}} f_2(\mathbf{F}) = \nabla_{\mathbf{F}} f_2(\mathbf{F}) - \text{Re}\{\nabla_{\mathbf{F}} f_2(\mathbf{F}) \odot \mathbf{F}\} \odot \mathbf{F}, \quad (47)$$

$$\text{grad}_{\mathbf{D}} f_3(\mathbf{D}) = \nabla_{\mathbf{D}} f_3(\mathbf{D}) - (\mathbf{I} \odot \text{Re}\{\mathbf{I} \odot (\nabla_{\mathbf{D}} f_3(\mathbf{D}))^H\}) \mathbf{D}. \quad (48)$$

Hence, the current point  $\boldsymbol{\theta}$ ,  $\mathbf{F}$ , and  $\mathbf{D}$  in the tangent space  $\mathcal{T}_{\boldsymbol{\theta}}\mathcal{M}_1$ ,  $\mathcal{T}_{\mathbf{F}}\mathcal{M}_2$ ,  $\mathcal{T}_{\mathbf{D}}\mathcal{M}_3$  are updated as  $\boldsymbol{\theta} - \delta_1 \nabla_{\boldsymbol{\theta}} f_1(\boldsymbol{\theta})$ ,  $\mathbf{F} - \delta_2 \nabla_{\mathbf{F}} f_2(\mathbf{F})$ , and  $\mathbf{D} - \delta_3 \nabla_{\mathbf{D}} f_3(\mathbf{D})$ , where  $\delta_1 > 0$ ,  $\delta_2 > 0$ , and  $\delta_3 > 0$  are the step size. It should be noticed that the update point may leave the manifold space. Thus, a retraction operation is used to ensure that the point stays in the manifold. More specifically the retraction operations are expressed as

$$\text{Ret}(\delta_1 \nabla_{\boldsymbol{\theta}} f_1(\boldsymbol{\theta})) = \frac{\boldsymbol{\theta} - \delta_1 \nabla_{\boldsymbol{\theta}} f_1(\boldsymbol{\theta})}{\|\boldsymbol{\theta} - \delta_1 \nabla_{\boldsymbol{\theta}} f_1(\boldsymbol{\theta})\|}, \quad (49)$$



$$\text{Ret}(\delta_2 \nabla_{\mathbf{F}} f_2(\mathbf{F})) = \frac{\mathbf{F} - \delta_2 \nabla_{\mathbf{F}} f_2(\mathbf{F})}{\|\mathbf{F} - \delta_2 \nabla_{\mathbf{F}} f_2(\mathbf{F})\|}, \quad (50)$$

$$\text{Ret}(\delta_3 \nabla_{\mathbf{D}} f_3(\mathbf{D})) = \frac{\mathbf{D} - \delta_3 \nabla_{\mathbf{D}} f_3(\mathbf{D})}{\|\mathbf{D} - \delta_3 \nabla_{\mathbf{D}} f_3(\mathbf{D})\|}. \quad (51)$$

Via these operations, we can obtain the solution for  $\Theta, \mathbf{F}, \mathbf{D}$ . The details are summarized in **Algorithm 2**. In the proposed AMO algorithm, the analog beamforming, the phase shifts of

---

**Algorithm 2:** Proposed AMO Algorithm for Problem (33)

---

- 1 **Intialization:** The iteration number  $t = 0$ ,  $t_1 = 0$ ,  $t_2 = 0$ ,  $t_3 = 0$ , the accuracy  $\epsilon_1$ ,  $\epsilon_2$ , and  $\epsilon_3$ .
  - 2 **Repeat:**
  - 3 **Repeat:**
  - 4 Calculate the Euclidean gradient and the Riemannian gradient based on (43) and (46)
  - 5 Determine the step size  $\delta_1^{t_1}$  based on [36], then, perform gradient descent algorithm over the current tangent space using  $\theta^{t_1} - \delta_1 \nabla_{\theta^{t_1}} f_1(\theta^{t_1})$  and update  $\theta$  based on (49)
  - 6 Set  $t_1 = t_1 + 1$ .
  - 7 **Until:**  $\|\theta^{t_1+1} - \theta^{t_1}\| \leq \epsilon_1$ .
  - 8 **Repeat:**
  - 9 Calculate the Euclidean gradient and the Riemannian gradient based on (44) and (47)
  - 10 Determine the step size  $\delta_2^{t_2}$  based on [36], then, perform gradient descent algorithm over the current tangent space using  $\mathbf{F}^{t_2} - \delta_2 \nabla_{\mathbf{F}^{t_2}} f_2(\mathbf{F}^{t_2})$  and update  $\mathbf{F}^{t_2}$  based on (50)
  - 11 Set  $t_2 = t_2 + 1$ .
  - 12 **Until:**  $\|f_2(\mathbf{F}^{t_2+1}) - f_2(\mathbf{F}^{t_2})\| \leq \epsilon_2$ .
  - 13 **Repeat:**
  - 14 Calculate the Euclidean gradient and the Riemannian gradient based on (45) and (48)
  - 15 Determine the step size  $\delta_3^{t_3}$  based on [36], then, perform gradient descent algorithm over the current tangent space using  $\mathbf{D}^{t_3} - \delta_3 \nabla_{\mathbf{D}^{t_3}} f_3(\mathbf{D}^{t_3})$  and update  $\mathbf{D}^{t_3}$  based on (51)
  - 16 Set  $t_3 = t_3 + 1$ .
  - 17 **Until:**  $\|f_3(\mathbf{D}^{t_3+1}) - f_3(\mathbf{D}^{t_3})\| \leq \epsilon_3$ .
  - 18 Set  $t = t + 1$ .
  - 19 **Until:** The stop condition is satisfied .
  - 20 **Output:**  $\theta^*, \mathbf{F}^*, \mathbf{D}^*$ .
-

the RIS, and the hybrid beamforming are optimized via the manifold optimization algorithm. According to **Theorem 4.3.1** in [36], the algorithm that uses the manifold optimization method is guaranteed to converge to the point where the gradient of the objective function is zero [36].

### B. Digital Beamforming Based on the SCA Algorithm

We assume that the hybrid beamforming matrix, the power allocation matrix, and the phase shift matrix of the RIS are fixed, and the digital beamforming in problem (30) is optimized. To simplify the writing of problem (30), we define the functions

$$f(\{z_{n,k,n}\}) = \sum_{n=1}^N \log_2(z_{n,k,n} \sum_{j=1}^k p_{n,j} + \sigma^2), \quad g(\{v_{n,k,i}\}) = -v_{n,k,i} v_{n,k,i}^H. \quad (52)$$

Also, (32a) can be re-written as

$$\begin{aligned} \min_{\mathbf{W}, \{\mathbf{u}_i\}, \{v_{n,k,i}\}, \{z_{n,k,i}\}} & \sum_{n=1}^N \sum_{k=1}^{|\mathcal{G}_n|} \log_2(z_{n,k,n} \sum_{j=1}^{k-1} p_{n,j} + \sigma^2) - \sum_{n=1}^N \sum_{k=1}^{|\mathcal{G}_n|} \log_2(z_{n,k,n} \sum_{j=1}^k p_{n,j} + \sigma^2) + \\ & \lambda \left( \sum_{i=1}^N \|\mathbf{u}_i - \mathbf{G}\mathbf{F}\mathbf{w}_i\|^2 + \|\mathbf{D} - \mathbf{F}\mathbf{W}\|^2 + \sum_{n=1}^N \sum_{k=1}^{|\mathcal{G}_n|} \sum_{i=1}^N \|v_{n,k,i} - \mathbf{h}_{n,k}^H \Theta \mathbf{u}_i\|^2 \right. \\ & \left. + \sum_{n=1}^N \sum_{k=1}^{|\mathcal{G}_n|} \sum_{i=1}^N (z_{n,k,i} - v_{n,k,i} v_{n,k,i}^H) \right), \end{aligned} \quad (53a)$$

$$\text{s.t. (26b), (26g), (31d).} \quad (53b)$$

The problem in (53) is a standard DC programming problem. However, it is still a non-convex problem. To deal with the non-convex objective function, we use the SCA method [35] in order to transform the non-convex part of the objective function into a convex function, and then to iteratively solve the convex approximation problem. In the following, we focus our attention on finding convex bounds for the concave functions  $f(\{z_{n,k,n}\})$  and  $g(\{v_{n,k,i}\})$ . To this end, the first-order Taylor expansion at the point  $(\{z_{n,k,n}\}, \{v_{n,k,i}\})$  can be written as

$$f(\{z_{n,k,n}\} | \{\tilde{z}_{n,k,n}\}) = f(\{\tilde{z}_{n,k,n}\} | \{\tilde{z}_{n,k,n}\}) + \sum_{n=1}^N \sum_{k=1}^{|\mathcal{G}_n|} \frac{\sum_{j=1}^k p_{n,j}}{\ln 2} \frac{z_{n,k,n} - \tilde{z}_{n,k,n}}{\tilde{z}_{n,k,n} \sum_{j=1}^k p_{n,j} + \sigma^2} \quad (54)$$

and

$$g(\{v_{n,k,i}\} | \{\tilde{v}_{n,k,i}\}) = \tilde{v}_{n,k,i} \tilde{v}_{n,k,i}^H - 2\text{Re}\{v_{n,k,i} \tilde{v}_{n,k,i}^H\}. \quad (55)$$

Therefore, the  $t + 1$ th iteration of the proposed SCA-based iterative algorithm is expressed as

$$\begin{aligned}
\min_{\mathbf{W}, \{\mathbf{u}_i\}, \{v_{n,k,i}\}, \{z_{n,k,i}\}} & \sum_{n=1}^N \sum_{k=1}^{|\mathcal{G}_n|} \log_2(\tilde{z}_{n,k,n}^t \sum_{j=1}^{k-1} p_{n,j} + \sigma^2) + \sum_{n=1}^N \sum_{k=1}^{|\mathcal{G}_n|} \frac{\sum_{j=1}^k p_{n,j} (z_{n,k,n} - \tilde{z}_{n,k,n}^t)}{\ln 2(\tilde{z}_{n,k,n}^t \sum_{j=1}^k p_{n,j} + \sigma^2)} \\
& - \sum_{n=1}^N \sum_{n=1}^N \sum_{k=1}^{|\mathcal{G}_n|} \log_2(z_{n,k,n} \sum_{j=1}^k p_{n,j} + \sigma^2) + \lambda \left( \sum_{i=1}^N \|\mathbf{u}_i - \mathbf{G}\mathbf{F}\mathbf{w}_i\|^2 \right. \\
& + \sum_{n=1}^N \sum_{k=1}^{|\mathcal{G}_n|} \sum_{i=1}^N \|v_{n,k,i} - \mathbf{h}_{n,k}^H \boldsymbol{\Theta} \mathbf{u}_i\|^2 + \|\mathbf{D} - \mathbf{F}\mathbf{W}\|^2 \\
& \left. + \sum_{n=1}^N \sum_{k=1}^{|\mathcal{G}_n|} \sum_{i=1}^N (z_{n,k,i} - \tilde{v}_{n,k,i}^t (\tilde{v}_{n,k,i}^H)^t + 2\text{Re}\{v_{n,k,i} (\tilde{v}_{n,k,i}^H)^t\}) \right) \quad (56a)
\end{aligned}$$

$$\text{s.t. (26b), (26g), (31d).} \quad (56b)$$

Starting with a feasible point for the problem (56), the proposed alternating optimization algorithm is summarized in **Algorithm 3**. The convergence of **Algorithm 3** is analyzed in the

---

**Algorithm 3:** Proposed SCA-based Algorithm for Problem (56)

---

- 1 **Initialization:**  $t = 0$ ,  $\{\tilde{v}_{n,k,j}^{(0)}\}, \{\tilde{z}_{n,k,j}^{(0)}\}$ ,  $\epsilon$  is the accuracy.
  - 2 **Repeat:**
  - 3 Calculating  $\{\mathbf{w}_n^{(t)}\}, \{v_{n,k,j}^{(t)}\}, \{z_{n,k,j}^{(t)}\}, \{\mathbf{u}_j^{(t)}\}$  by using CVX [35].
  - 4 Update  $\tilde{v}_{n,k,j}^{(t+1)} = v_{n,k,j}^{(t)}$ ,  $\tilde{z}_{n,k,j}^{(t+1)} = z_{n,k,j}^{(t)}$ .
  - 5 Set  $t = t + 1$ ;
  - 6 **Until:**  $\|\mathbf{w}_n^{(t)} - \mathbf{w}_n^{(t-1)}\|^2 \leq \epsilon$ .
  - 7 **Output:**  $\mathbf{W}^*$
- 

following theorem.

**Theorem 4.** *Algorithm 3 converges to a stationary point that satisfies the KKT conditions.*

*The proof is given in Appendix D.*

### C. Optimization Algorithms to Solve (14) and Computational Complexity

In the above sections, we have presented the algorithms for power allocation, digital beamforming, analog beamforming, and phase shifts optimization. Based on these algorithms. **Algorithm 4** provides the proposed solution for solving the general optimization problem in (14). In particular,

we first use **Algorithm 1** to solve the power allocation problem, and we assume that the hybrid beamforming matrix and phase shifts of the RIS are fixed. Thus, the power allocation can be viewed as the function of the power matrix. Then, we calculate the analog beamforming and phase shifts of the RIS by using **Algorithm 2**. Finally, the digital beamforming matrix is obtained by using **Algorithm 3**.

---

**Algorithm 4:** Proposed J-PA-HB-PSO Algorithm for Problem (12)

---

- 1 **Initialization:**  $\{p_{m,k}^{(0)}\}$ ,  $\{P_m^{(0)}\}$ ,  $\Theta^{(0)}$ ,  $\mathbf{W}^{(0)}$ ,  $\mathbf{F}^{(0)}$ .
  - 2 **Repeat:**
  - 3 Using **Algorithm1** to calculate  $\{p_{m,k}^{(t)}\}$  and  $\{P_m^{(t)}\}$ .
  - 4 Using **Algorithm2** to calculate  $\Theta^{(t)}$  and  $\mathbf{F}^{(t)}$ .
  - 5 Using **Algorithm3** to calculate  $\mathbf{W}^{(t)}$ .
  - 6 Reorder the effective channel gains of the users in each group.
  - 7 Set  $t = t + 1$ .
  - 8 **Until:**  $p_{m,k}^{(t)} = p_{m,k}^{(t+1)}$ ,  $P_m^{(t)} = P_m^{(t+1)}$ ,  $\Theta^{(t)} = \Theta^{(t+1)}$ , and  $\mathbf{W}^{(t)} = \mathbf{W}^{(t+1)}$ .
  - 9 **Output:**  $\{p_{n,k}^*\}$ ,  $\{P_n^*\}$ ,  $\Theta^*$ ,  $\mathbf{W}^*$ ,  $\mathbf{F}^*$ .
- 

In **Algorithm 1**, the complexity of calculating the effective channel gains of the users is  $\mathcal{O}(MKN)$ . Each time that  $\{P_m\}$  is updated, the maximum number of iterations is  $M$ , and the complexity of computing  $\{P_m\}$  in each subcycle is no higher than  $\mathcal{O}(K^2)$ . Thus, the complexity of **Algorithm 1** is  $\mathcal{O}(MKN + S_1MK^2)$ , where  $S_1$  is the number of iterations. In **Algorithm 2**, according to [37], the computational complexity of the AMO algorithm is  $\mathcal{O}(T_1 \frac{1}{\epsilon_1^2} + T_2 \frac{1}{\epsilon_2^2} + T_3 \frac{1}{\epsilon_3^2})$ , where  $T_1$ ,  $T_2$  and  $T_3$  are the number of iterations. The transmit beamforming problem in (56) is solved by using **Algorithm 3** that is based on the SCA method. Since there are  $2N_tN_{RF} + 2N_rK + 3NK^2$  real variables in problem (56), the computational complexity of the SCA method is  $\mathcal{O}(S_3(2N_tN_{RF} + 2N_rK + 3NK^2)^{3.5} \log_2(\frac{1}{\epsilon}))$  according to [38], where  $\epsilon$  is the accuracy of the SCA method and  $S_3$  is the number of iterations. Therefore, the computational complexity of **Algorithm 4** is  $\mathcal{O}(T(MKN + S_1MK^2 + S_3(2N_tN_{RF} + 2N_rK + 3NK^2)^{3.5} \log_2(\frac{1}{\epsilon}) + T_1 \frac{1}{\epsilon_1^2} + T_2 \frac{1}{\epsilon_2^2} + T_3 \frac{1}{\epsilon_3^2}))$ , where  $T$  is the number of iterations of **Algorithm 4**.

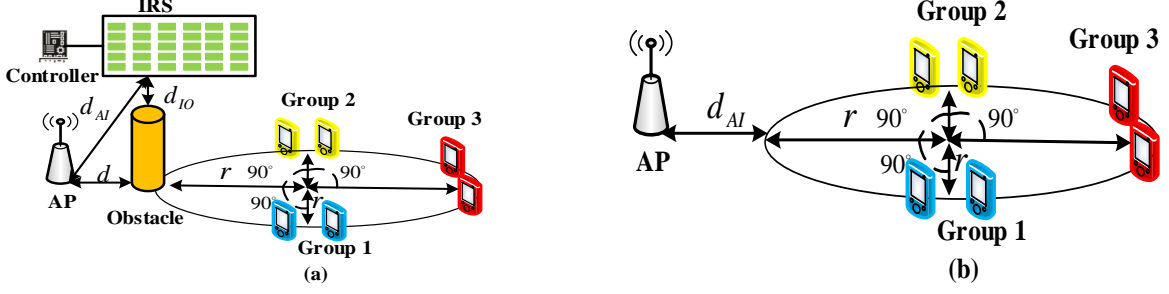


Fig. 2. Simulated RIS-aided mmWave-NOMA communication scenario in (a). Simulated mmWave-NOMA communication scenario without RIS in (b).

## V. NUMERICAL RESULTS

In this section, simulation results are provided to verify the performance of the considered RIS-aided mmWave-NOMA system. The simulation scenario is shown in Fig. 2, where the obstacles and three groups of users are distributed on a circle with a radius of  $r = 50$  m. The RIS and the obstacle locate on a line and the distance between them is  $d_{IO} = 9$  m. The AP and the obstacle are also on the same line and the distance between them is  $d = 16$  m. The distance between the AP and the RIS is 25 m. The channel models in (5) and (6) are considered. Based on [30], the path fading factor  $\alpha$  and  $\beta_{n,k}$  satisfy the Gaussian distribution  $\mathcal{CN}(0, 10^{-PL_\alpha(d_{AI})})$  and  $\mathcal{CN}(0, 10^{-PL_{\beta_{n,k}}(d_{Ik})})$ , where  $d_{Ik}$  represents the distance from the RIS to the  $k$  user. According to [30],  $PL_\alpha(d_{AI})$  and  $PL_{\beta_{n,k}}(d_{Ik})$  can be formulated as follows

$$PL_\alpha(d_{AI}) = \eta_a + 10\eta_b \log_{10}(d_{AI}) + \beta \quad (57)$$

$$PL_{\beta_{n,k}}(d_{Ik}) = \eta_a + 10\eta_b \log_{10}(d_{Ik}) + \beta, \quad (58)$$

where  $\beta \sim \mathcal{CN}(0, \sigma_\beta^2)$  is the variance of the shadowing.  $\eta_a = 73$ ,  $\eta_b = 2.92$  and  $\sigma_\beta = 8.7$  dB. The other parameters are set as follows:  $N_t = 32$ ,  $N_{RF} = N = 3$ ,  $K = 6$ ,  $N_r = 64$ . The transmit power is  $P = 30$  dBm and the noise power is  $\sigma^2 = 1$  mW. For comparison and benchmarking, four different transmission schemes are considered: a mmWave-NOMA scheme without RIS, an RIS-aided all-digital structure mmWave-NOMA system, an all-digital structure mmWave-NOMA system without RIS, and a mmWave-FDMA scheme without RIS. The system setup without RIS is illustrated in Fig. 2(b).

In Figs. 3, the convergence of the proposed algorithms is analyzed by using numerical simulations. In the figures, the power allocation algorithm is called the first layer iteration, the manifold

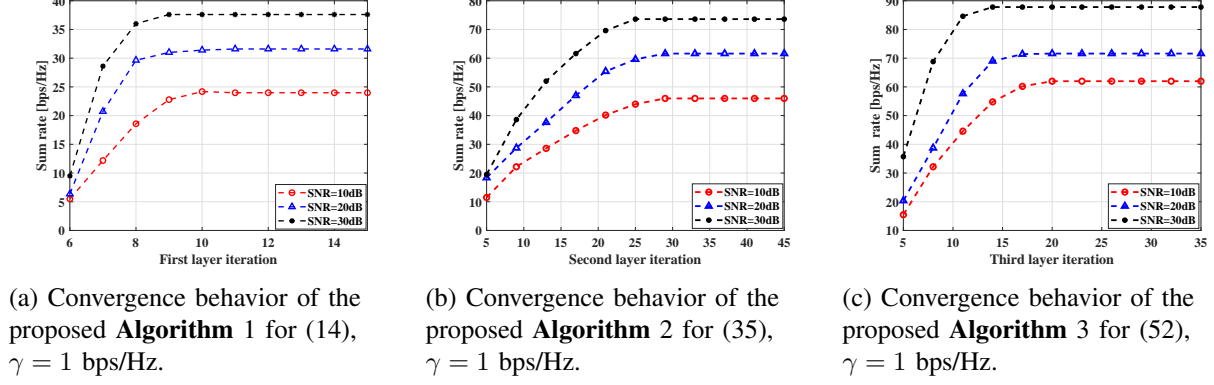


Fig. 3. Convergence behavior of the proposed algorithms.

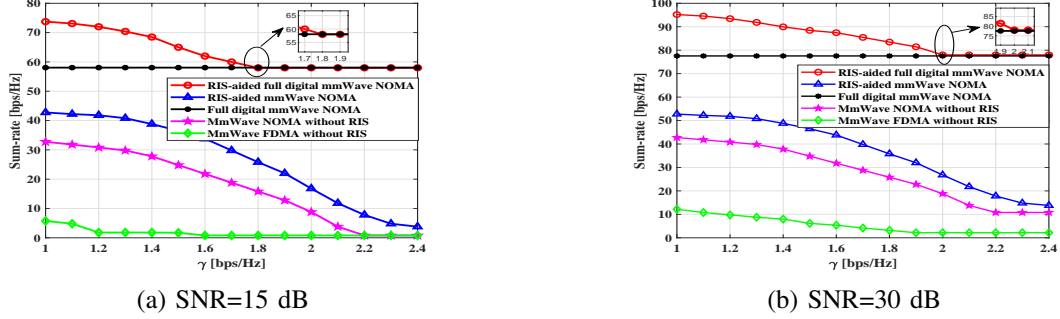


Fig. 4. Sum-rate versus minimum rate constraint of user.

optimization algorithm is called the second layer iteration, and the SCA-based algorithm is called the third iteration. In Fig. 3(a), the convergence of the algorithm against the number of iterations is studied, and it is observed that the sum-rate of the power allocation algorithm converges in about 10 iterations. The simulation results in Fig. 3(b) and Fig. 3(c) show that the phase shifts optimization based on the AMO algorithm and the transmit beamforming optimization based on SCA algorithm have good convergence performance. The sum-rate increases with the increase of the SNR and finally converges to a stable value.

Fig. 4 compares the sum-rate of all of the considered transmission schemes. The minimum rate constraint for all the users is equal to  $\gamma$ . The proposed RIS-aided hybrid mmWave-NOMA system outperforms the hybrid mmWave-OMA system without the RIS. Similarly, the RIS-aided fully-digital mmWave-NOMA system outperforms the fully-digital mmWave-OMA system without the RIS. When the minimum rate constraint  $\gamma$  is small, e.g., 1 bps, proposed RIS-aided schemes largely outperform the schemes without RIS. When  $\gamma$  is small, in fact, more power can be

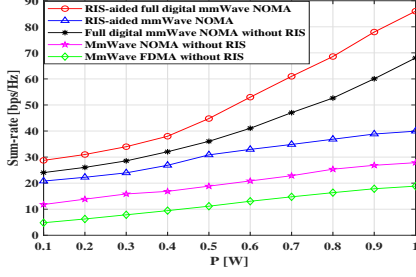
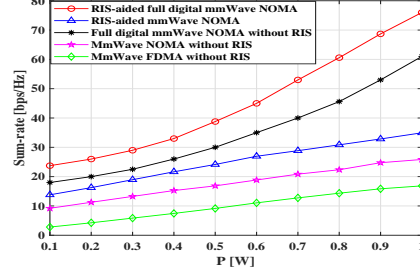
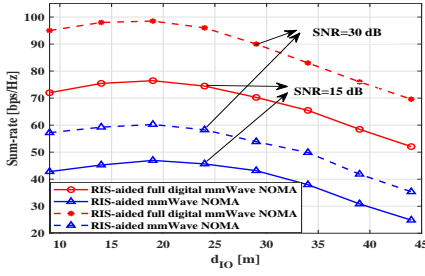
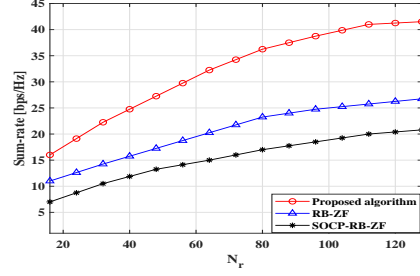
(a)  $\gamma = 1$  bps/Hz(b)  $\gamma = 1.5$  bps/Hz

Fig. 5. Sum-rate versus total power.

(a)  $P = 30$  dBm,  $\gamma = 1$  bps/Hz(b)  $\gamma = 1.5$  bps/Hz,  $P = 0.5$  W.Fig. 6. Sum-rate of the users versus the distance  $d_{IO}$  for different SNR in (a), sum-rate versus the number of phase shifts of RIS in (b).

allocated to the users with the highest channel gain in each group by appropriately optimizing the phase shifts of the RIS. Moreover, there exist channel realizations that can not satisfy the minimum rate constraint when  $\gamma$  is large. In this case, the rate is set equal to zero. We note that the sum-rate of the proposed RIS-aided schemes is close to that of all-digital mmWave NOMA schemes without RIS, which highlights that the proposed RIS-based schemes can suppress the interference well.

Fig. 5 shows the sum-rate of the four considered schemes as a function of the total transmission power. From Fig. 5, it can be found that the proposed RIS-aided hybrid mmWave-NOMA and RIS-aided fully-digital mmWave-NOMA schemes can achieve a higher sum-rate than the RIS-aided hybrid mmWave-NOMA and fully-digital mmWave-NOMA systems. In particular, when the transmission power is low, the superiority RIS-aided schemes is more apparent.

In Fig. 6(a), we plot the sum-rate of the users against the distance from the RIS to the obstacle for different SNR, which allows us to examine the impact of the distance on the system

performance. We compare the performance of the proposed RIS-aided full digital mmWave NOMA scheme with that of RIS-aided mmWave NOMA scheme. We observe that the sum-rate of the users first increases with the distance  $d_{IO}$  and then decreases when  $d_{IO}$  is beyond a certain value. This is attributed to the fact that the desired signal and the interference received by the users decrease when  $d_{IO}$  increases. However, the attenuation of the interference is larger than that of desired signal because the interference undergoes a more severe path loss. As  $d_{IO}$  further increases, the desired signal strength further decreases, which decreases the sum-rate of the users. Furthermore, we observe that the performance gain of all the proposed RIS-aided schemes increase when  $d_{IO}$  decreases. In this situation, the optimization of the location of the RIS becomes critical.

In Fig. 6(b), the performance of the proposed optimization scheme as a function of the number of RIS elements is evaluated. For comparison, the performance of two benchmark schemes is considered as well. The first benchmark scheme (called RB-ZF in the figure) corresponds to using random phases for the phase shifts of the RIS and for analog beamforming, as well as zero-forcing (ZF) for digital beamforming, [39]. The second benchmark scheme corresponds to using (called COCP-RB-ZF in the figure), analog beamforming with random phase shift and digital precoding used ZF, [40]. Fig. 6b shows that the proposed RIS-based scheme has better performance than the other schemes. In all cases, as expected, the performance improves with the increase of the number of RIS reflection elements. It is worth noting that the RB-ZF and the COCP RB-ZF schemes do not account for the impact of interference from other groups. This is one of the reasons of the superiority of the proposed scheme.

## VI. CONCLUSION

In this paper, the joint power allocation, phase shifts optimization, and hybrid beamforming design for downlink multiuser RIS-aided mmWave-NOMA was investigated. The phase shifts of the RIS, the power allocation at the AP, and the hybrid beamforming were jointly optimized for maximizing the system sum-rate. To solve the corresponding non-convex problem, we proposed a J-PA-HB-PSO algorithm. First, a sub-optimal algorithm is proposed for power allocation under arbitrarily fixed phase shifts and hybrid beamforming. Then, given the power allocation, we utilized the AMO algorithm and SCA-based algorithm to design the phase shifts of the RIS and the hybrid beamforming to maximize the sum-rate. Finally, numerical results showed that the proposed algorithms are capable of achieving near-optimal performance and that a significant



performance gain can be achieved by optimizing the phase shifts of the RIS. In addition, simulation results showed that the proposed RIS-aided mmWave-NOMA scheme outperforms mmWave-NOMA schemes without the RIS.

## APPENDIX A

### PROOF OF THEOREM 1

Because the interference from other groups is ignored, the SINR for user 1 in group  $n$  can be written as follows

$$f_{n,1} = \frac{|\mathbf{h}_{n,1}^H \mathbf{\Theta} \mathbf{G} \mathbf{F} \mathbf{w}_n|^2 p_{n,1}}{\sigma^2}. \quad (65)$$

Based on  $\sum_{k=1}^{|\mathcal{G}_n|} p_{n,k} = P_n$ , the relationship between  $p_{n,1}$  and  $P_n$  is linear. Therefore, the relationship between  $\gamma_{n,1}$  and  $P_n$  is

$$f_{n,1} = \beta_n P_n + \alpha_n, \quad (66)$$

where  $\beta_n$  and  $\alpha_n$  are expressed as

$$\beta_n = \frac{|\mathbf{h}_{n,1}^H \mathbf{\Theta} \mathbf{G} \mathbf{F} \mathbf{w}_n|^2}{\sigma^2} \left( 1 - \sum_{k=2}^{|\mathcal{G}_n|} \left[ (2^{\gamma_{n,k}} - 1) \prod_{j=2}^k \frac{1}{2^{\gamma_{n,j}}} \right] \right), \quad (67)$$

$$\alpha_n = -\frac{|\mathbf{h}_{n,1}^H \mathbf{\Theta} \mathbf{G} \mathbf{F} \mathbf{w}_n|^2}{\sigma^2} \sum_{k=2}^{|\mathcal{G}_n|} \left[ (2^{\gamma_{n,k}} - 1) \frac{\sigma^2}{|\mathbf{h}_{n,k}^H \mathbf{\Theta} \mathbf{G} \mathbf{F} \mathbf{w}_k|^2} \prod_{j=2}^k \frac{1}{2^{\gamma_{n,j}}} \right]. \quad (68)$$

It is not difficult to find that  $\beta_n \geq 0$  and  $\alpha_n \geq 0$ . Then, (20a) and (14b) are rewritten as

$$\sum_{n=1}^N \log_2(\beta_n P_n + \alpha_n + 1), \quad \eta_{n,1} - \alpha_n - P_n \beta_n \leq 0. \quad (69)$$

According to (69), the problem in (20) can be stated as

$$\max_{\{P_n\}} \sum_{n=1}^N R_{n,1}, \quad (70a)$$

$$\text{s.t. } \eta_{n,1} - \alpha_n - P_n \beta_n \leq 0, \quad \sum_{n=1}^N P_n \leq 0, \quad (70b)$$

We denote the objective function in (20a) as  $f(\{P_n\}) = \sum_{n=1}^N \log_2(\beta_n P_n + \alpha_n)$ . We observe that  $f(\{P_n\})$  is an increasing function in  $P_n$ . Ignoring the constraint (14b), problem (20) can be

solved by the Karush-Kuhn-Tucker (KKT) conditions, i.e.,

$$\frac{\partial f(\{P_n\})}{\partial P_n} = \lambda, \quad \sum_{n=1}^N P_n = P. \quad (71)$$

The solution of equation in (71) is

$$\bar{P}_n = \frac{P}{N} - \frac{\alpha_n + 1}{\beta_n} + \sum_{i=1}^N \frac{\alpha_i + 1}{N\beta_i}. \quad (72)$$

Then, **Theorem 1** is proved.

## APPENDIX B

### PROOF OF **THEOREM 2**

To prove **Theorem 2**, we use the method of proof by contradiction. Assuming there is an optimal solution  $\hat{P}_{n_1}$  which satisfies  $\hat{P}_{n_1} > \frac{2^{\gamma_{n_1,1}} - \alpha_{n_1}}{\beta_{n_1}} > \bar{P}_{n_1}$ . Since  $\sum_{n=1}^N \hat{P}_n \leq P$ , there always exists  $\hat{P}_{n_2} \leq \bar{P}_{n_2}$  ( $n_2 \neq n_1$ ). The power allocation solution can be expressed as

$$L_{n_1} = \hat{P}_{n_1} - \delta, \quad L_{n_2} = \hat{P}_{n_2} + \delta, \quad L_n = \hat{P}_n, n \neq n_1, n_2. \quad (73)$$

Therefore, we only need to prove that the sum rate of the power allocation solution  $\{L_n\}$  is higher than that of the solution  $\{\hat{P}_n\}$ . We assume that the objective function in (20a) with solution  $\{L_n\}$  is  $g(\{L_n\}) = \sum_{n=1}^N \log_2(\beta_n L_n + \alpha_n)$ , and the objective function in (20a) with solution  $\{\hat{P}_n\}$  is  $h(\{\hat{P}_n\}) = \sum_{n=1}^N \log_2(\beta_n \hat{P}_n + \alpha_n)$ . If  $\delta = 0$ , then  $g(\{L_n\}) - h(\{\hat{P}_n\}) = 0$ . The derivative of  $g(\{L_n\}) - h(\{\hat{P}_n\})$  with respect to  $\delta$  is

$$\frac{\partial g(\{L_n\}) - h(\{\hat{P}_n\})}{\partial \delta} = \frac{1}{\ln 2} \frac{\beta_{n_2}}{(\beta_{n_2}(\hat{P}_{n_2} + \delta) + \alpha_{n_2} + 1)} - \frac{1}{\ln 2} \frac{\beta_{n_1}}{(\beta_{n_1}(\hat{P}_{n_1} - \delta) + \alpha_{n_1} + 1)}. \quad (74)$$

According to the derivative of the objective function (20a), we have

$$\frac{1}{\ln 2} \frac{\beta_{n_2}}{(\beta_{n_2}(\hat{P}_{n_2} + \delta) + \alpha_{n_2} + 1)} > \frac{1}{\ln 2} \frac{\beta_{n_2}}{(\beta_{n_2}\bar{P}_{n_2} + \alpha_{n_2} + 1)} \quad (75)$$

$$\frac{1}{\ln 2} \frac{\beta_{n_1}}{(\beta_{n_1}(\hat{P}_{n_1} - \delta) + \alpha_{n_1} + 1)} < \frac{1}{\ln 2} \frac{\beta_{n_1}}{(\beta_{n_1}\bar{P}_{n_1} + \alpha_{n_1} + 1)}, \quad (76)$$

where  $\frac{1}{\ln 2} \frac{\beta_{n_1}}{(\beta_{n_1}\bar{P}_{n_1} + \alpha_{n_1} + 1)} = \frac{1}{\ln 2} \frac{\beta_{n_2}}{(\beta_{n_2}\bar{P}_{n_2} + \alpha_{n_2} + 1)} = \frac{1}{\ln 2} \frac{N}{P + \sum_{n=1}^N \frac{\alpha_n + 1}{\beta_n}}$ . Therefore, (72) is equivalent to

$$\frac{\partial g(\{L_n\}) - h(\{\hat{P}_n\})}{\partial \delta} > \frac{1}{\ln 2} \frac{\beta_{n_2}}{(\beta_{n_2}\bar{P}_{n_2} + \alpha_{n_2} + 1)} - \frac{1}{\ln 2} \frac{\beta_{n_1}}{(\beta_{n_1}\bar{P}_{n_1} + \alpha_{n_1} + 1)} = 0. \quad (77)$$

Since  $g(\{L_n\}) - h(\{\hat{P}_n\}) = 0$ , we have  $g(\{L_n\}) > h(\{\hat{P}_n\})$ , which demonstrates that  $\{L_n\}$  is better than  $\{\hat{P}_n\}$ . This contradicts the assumption that  $\{\hat{P}_n\}$  is the optimal solution. To this end, the optimal solution of problem (20) must satisfy  $\hat{P}_n = \frac{2^{\gamma_{n,1} - \alpha_n}}{\beta_n}$ ,  $n \in \mathcal{N}$ . Thus, **Theorem 2** is proved.

## APPENDIX C

### PROOF OF THEOREM 3

According to the Schur complement,  $\begin{bmatrix} z_{n,k,i} & v_{n,k,i} \\ v_{n,k,i}^H & 1 \end{bmatrix} \succeq \mathbf{0}$  is equivalent to  $z_{n,k,i} - v_{n,k,i} v_{n,k,i}^H > 0$ . Combining  $z_{n,k,i} - v_{n,k,i} v_{n,k,i}^H > 0$  with  $z_{n,k,i} - v_{n,k,i} v_{n,k,i}^H < 0$ , we have  $z_{n,k,i} - v_{n,k,i} v_{n,k,i}^H = 0$ , thus,  $z_{n,k,i} = v_{n,k,i} v_{n,k,i}^H$ , which demonstrates that we can replace (30f) with (33) and (34). Thus **Theorem 3** is proved.

## APPENDIX D

### PROOF OF THEOREM 4

In order to simplify the notation, let  $Q(\{\mathbf{w}_i\}, \{\mathbf{u}_i\}, \{v_{n,k,i}\}, \{z_{n,k,i}\})$  denote (57a) and  $Q(\{\mathbf{w}_i\}, \{\mathbf{u}_i\}, \{v_{n,k,i}\}, \{z_{n,k,i}\} | \{\tilde{v}_{n,k,i}\}, \{\tilde{z}_{n,k,i}\})$  denote (60a). In each iteration of **Algorithm 4**,  $Q(\{\mathbf{w}_i\}, \{\mathbf{u}_i\}, \{v_{n,k,i}\}, \{z_{n,k,i}\})$  is replaced by  $Q(\{\mathbf{w}_i\}, \{\mathbf{u}_i\}, \{v_{n,k,i}\}, \{z_{n,k,i}\} | \{\tilde{v}_{n,k,i}\}, \{\tilde{z}_{n,k,i}\})$ , which is a differentiable convex function. Based on [41], **Algorithm 4** converges to a KKT point of the problem (58), which must satisfy the following conditions:

$$Q(\{\mathbf{w}_i\}, \{\mathbf{u}_i\}, \{v_{n,k,i}\}, \{z_{n,k,i}\}) \leq Q(\{\mathbf{w}_i\}, \{\mathbf{u}_i\}, \{v_{n,k,i}\}, \{z_{n,k,i}\} | \{\tilde{v}_{n,k,i}\}, \{\tilde{z}_{n,k,i}\}) \quad (78)$$

$$Q(\{\mathbf{w}_i^t\}, \{\mathbf{u}_i^t\}, \{v_{n,k,i}^t\}, \{z_{n,k,i}^t\}) = Q(\{\mathbf{w}_i^t\}, \{\mathbf{u}_i^t\}, \{v_{n,k,i}^t\}, \{z_{n,k,i}^t\} | \{\tilde{v}_{n,k,i}^{t+1}\}, \{\tilde{z}_{n,k,i}^{t+1}\}) \quad (79)$$

$$\frac{\partial Q(\{\mathbf{w}_i^t\}, \{\mathbf{u}_i^t\}, \{v_{n,k,i}^t\}, \{z_{n,k,i}^t\})}{\partial v_{n,k,i}} = \frac{\partial Q(\{\mathbf{w}_i^t\}, \{\mathbf{u}_i^t\}, \{v_{n,k,i}^t\}, \{z_{n,k,i}^t\} | \{\tilde{v}_{n,k,i}^{t+1}\}, \{\tilde{z}_{n,k,i}^{t+1}\})}{\partial v_{n,k,i}} \quad (80)$$

$$\frac{\partial Q(\{\mathbf{w}_i^t\}, \{\mathbf{u}_i^t\}, \{v_{n,k,i}^t\}, \{z_{n,k,i}^t\})}{\partial z_{n,k,i}} = \frac{\partial Q(\{\mathbf{w}_i^t\}, \{\mathbf{u}_i^t\}, \{v_{n,k,i}^t\}, \{z_{n,k,i}^t\} | \{\tilde{v}_{n,k,i}^{t+1}\}, \{\tilde{z}_{n,k,i}^{t+1}\})}{\partial z_{n,k,i}}. \quad (81)$$

According to the Taylor expansion,  $Q(\{\mathbf{w}_i\}, \{\mathbf{u}_i\}, \{v_{n,k,i}\}, \{z_{n,k,i}\})$  and  $Q(\{\mathbf{w}_i\}, \{\mathbf{u}_i\}, \{v_{n,k,i}\}, \{z_{n,k,i}\} | \{\tilde{v}_{n,k,i}\}, \{\tilde{z}_{n,k,i}\})$  satisfy the first condition. Since  $\tilde{v}_{n,k,i}^{t+1} = v_{n,k,i}^t$  and  $\tilde{z}_{n,k,i}^{t+1} = z_{n,k,i}^t$ , the second condition is satisfied as well. Finally, we verify the conditions in (80)-(81) by deriving the first derivatives of  $Q(\{\mathbf{w}_i^t\}, \{\mathbf{u}_i^t\}, \{v_{n,k,i}^t\}, \{z_{n,k,i}^t\})$  and  $Q(\{\mathbf{w}_i^t\}, \{\mathbf{u}_i^t\}, \{v_{n,k,i}^t\}, \{z_{n,k,i}^t\} | \{\tilde{v}_{n,k,i}^{t+1}\}, \{\tilde{z}_{n,k,i}^{t+1}\})$  with respect to  $v_{n,k,i}$  and  $z_{n,k,i}$ , respectively. They can be written as follows:

$$\frac{\partial Q(\{\mathbf{w}_i^t\}, \{\mathbf{u}_i^t\}, \{v_{n,k,i}^t\}, \{z_{n,k,i}^t\})}{\partial v_{n,k,i}} = \lambda((v_{n,k,i}^t)^* - ((\mathbf{h}_{n,k}^t)^H \boldsymbol{\Theta}^t \mathbf{u}_i^t)^* - (v_{n,k,i}^t)^*). \quad (82)$$

$$\frac{\partial Q(\{\mathbf{w}_i^t\}, \{\mathbf{u}_i^t\}, \{v_{n,k,i}^t\}, \{z_{n,k,i}^t\} | \{\tilde{v}_{n,k,i}^{t+1}\}, \{\tilde{z}_{n,k,i}^{t+1}\})}{\partial v_{n,k,i}} = \lambda((v_{n,k,i}^t)^* - ((\mathbf{h}_{n,k}^t)^H \boldsymbol{\Theta}^t \mathbf{u}^t)^* - (v_{n,k,i}^t)^*). \quad (83)$$

$$\frac{\partial Q(\{\mathbf{w}_i^t\}, \{\mathbf{u}_i^t\}, \{v_{n,k,i}^t\}, \{z_{n,k,i}^t\})}{\partial z_{n,k,i}} = \begin{cases} \frac{\sum_{j=1}^{k-1} p_{n,j}}{\ln_2(z_{n,k,n}^t \sum_{j=1}^{k-1} p_{n,j} + \sigma^2)} - \frac{\sum_{j=1}^k p_{n,j}}{\ln_2(z_{n,k,n}^t \sum_{j=1}^k p_{n,j} + \sigma^2)} & n = i \\ 1 & n \neq i. \end{cases} \quad (84)$$

$$\frac{\partial Q(\{\mathbf{w}_i^t\}, \{\mathbf{u}_i^t\}, \{v_{n,k,i}^t\}, \{z_{n,k,i}^t\} | \{\tilde{v}_{n,k,i}^{t+1}\}, \{\tilde{z}_{n,k,i}^{t+1}\})}{\partial z_{n,k,i}} = \begin{cases} \frac{\sum_{j=1}^{k-1} p_{n,j}}{\ln_2(z_{n,k,n}^t \sum_{j=1}^{k-1} p_{n,j} + \sigma^2)} - \frac{\sum_{j=1}^k p_{n,j}}{\ln_2(z_{n,k,n}^t \sum_{j=1}^k p_{n,j} + \sigma^2)} & n = i \\ 1 & n \neq i. \end{cases} \quad (85)$$

The conditions (20) and (21) are verified to be satisfied. Therefore, **Algorithm 4** converges to a KKT solution of problem (58).

## REFERENCES

- [1] W. Roh, J.-Y. Seol, J. Park, B. Lee, J. Lee, Y. Kim, J. Cho, K. Cheun, and F. Aryanfar, “Millimeter-wave beamforming as an enabling technology for 5G cellular communications: Theoretical feasibility and prototype results,” *IEEE Commun. Mag.*, vol. 52, no. 2, pp. 106–113, Feb. 2014.
- [2] P. Wang, Y. Li, L. Song, and B. Vucetic, “Multi-gigabit millimeter wave wireless communications for 5G: From fixed access to cellular networks,” *IEEE Commun. Mag.*, vol. 53, no. 1, pp. 168–178, Jan. 2015.
- [3] M. Di Renzo, A. Zappone, M. Debbah, M.-S. Alouini, C. Yuen, J. de Rosny, and S. Tretyakov, “Smart radio environments empowered by reconfigurable intelligent surfaces: How it works, state of research, and road ahead,” *arXiv preprint arXiv:2004.09352*, 2020.
- [4] L. Dai, B. Wang, M. Peng, and S. Chen, “Hybrid precoding-based millimeter-wave massive MIMO-NOMA with simultaneous wireless information and power transfer,” *IEEE J. Sel. Areas Commun.*, vol. 37, no. 1, pp. 131–141, Jan. 2019.
- [5] Z. Xiao, L. Zhu, J. Choi, P. Xia, and X.-G. Xia, “Joint power allocation and beamforming for non-orthogonal multiple access (NOMA) in 5G millimeter wave communications,” *IEEE Trans. Wireless Commun.*, vol. 17, no. 5, pp. 2961–2974, May. 2018.
- [6] L. Dai, B. Wang, Z. Ding, Z. Wang, S. Chen, and L. Hanzo, “A survey of non-orthogonal multiple access for 5G,” *IEEE commun. surveys tutorials.*, vol. 20, no. 3, pp. 2294–2323, Dec. 2018.
- [7] M. Liu, T. Song, and G. Gui, “Deep cognitive perspective: Resource allocation for NOMA-based heterogeneous IoT with imperfect SIC,” *IEEE Internet of Things J.*, vol. 6, no. 2, pp. 2885–2894, Dec. 2018.
- [8] A. Alkhateeb, G. Leus, and R. W. Heath, “Limited feedback hybrid precoding for multi-user millimeter wave systems,” *IEEE Trans. Wireless Commun.*, vol. 14, no. 11, pp. 6481–6494, Nov. 2015.

- [9] Q. Wu and R. Zhang, "Towards smart and reconfigurable environment: Intelligent reflecting surface aided wireless network," *IEEE Commun. Mag.*, vol. 58, no. 1, pp. 106–112, Jan. 2020.
- [10] X. Guan, Q. Wu, and R. Zhang, "Joint power control and passive beamforming in ired-assisted spectrum sharing," *IEEE Commun. Lett.*, vol. 24, no. 7, pp. 1553–1557, Jul. 2020.
- [11] Q. Wu and R. Zhang, "Intelligent reflecting surface enhanced wireless network via joint active and passive beamforming," *IEEE Trans. Wireless Commun.*, vol. 18, no. 11, pp. 5394–5409, Nov. 2019.
- [12] H. Guo, Y.-C. Liang, J. Chen, and E. G. Larsson, "Weighted sum-rate optimization for intelligent reflecting surface enhanced wireless networks," *arXiv preprint arXiv:1905.07920*, 2019.
- [13] Y. Cao and T. Lv, "Intelligent reflecting surface enhanced resilient design for MEC offloading over millimeter wave links," *arXiv preprint arXiv:1912.06361*, 2019.
- [14] V. Jamali, A. Tulino, G. Fischer, R. Müller, and R. Schober, "Intelligent reflecting and transmitting surface aided millimeter wave massive mimo," [Online] Available: <https://arxiv.org/abs/1902.07670>, 2019, 2019.
- [15] C. Pradhan, A. Li, L. Song, B. Vucetic, and Y. Li, "Hybrid precoding design for reconfigurable intelligent surface aided mmwave communication systems," *IEEE Wireless Commun. Lett.*, vol. 9, no. 7, pp. 1041–1045, Jul. 2020.
- [16] P. Wang, J. Fang, X. Yuan, Z. Chen, H. Duan, and H. Li, "Intelligent reflecting surface-assisted millimeter wave communications: Joint active and passive precoding design," *arXiv preprint arXiv:1908.10734*, 2019.
- [17] J. Zhu, Y. Huang, J. Wang, K. Navaie, and Z. Ding, "Power efficient IRS-assisted NOMA," *arXiv preprint arXiv:1912.11768*, 2019.
- [18] B. Zheng, Q. Wu, and R. Zhang, "Intelligent reflecting surface-assisted multiple access with user pairing: NOMA or OMA?" *IEEE Commun. Lett.*, vol. 24, no. 4, pp. 753–757, Apr. 2020.
- [19] J. Zuo, Y. Liu, Z. Qin, and N. Al-Dhahir, "Resource allocation in intelligent reflecting surface assisted NOMA systems," *arXiv preprint arXiv:2002.01765*, 2020.
- [20] M. Zeng, X. Li, G. Li, W. Hao, and O. Dobre, "Sum rate maximization for IRS-assisted uplink NOMA," *arXiv preprint arXiv:2004.10791*, 2020.
- [21] G. Zhou, C. Pan, H. Ren, K. Wang, M. Di Renzo, and A. Nallanathan, "Robust beamforming design for intelligent reflecting surface aided miso communication systems," *IEEE Wireless Commun. Lett.*, Early Access. 2020.
- [22] X. Qian, M. Di Renzo, J. Liu, A. Kammoun, and M.-S. Alouini, "Beamforming through reconfigurable intelligent surfaces in single-user mimo systems: SNR distribution and scaling laws in the presence of channel fading and phase noise," *arXiv preprint arXiv:2005.07472*, 2020.
- [23] R. Karasik, O. Simeone, M. Di Renzo, and S. Shamai, "Beyond max-SNR: Joint encoding for reconfigurable intelligent surfaces," *arXiv preprint arXiv:1911.09443*, 2019.
- [24] N. S. Perović, M. Di Renzo, and M. F. Flanagan, "Channel capacity optimization using reconfigurable intelligent surfaces in indoor mmwave environments," *arXiv preprint arXiv:1910.14310*, 2019.
- [25] S. Liu, Z. Gao, J. Zhang, M. Di Renzo, and M.-S. Alouini, "Deep denoising neural network assisted compressive channel estimation for mmwave intelligent reflecting surfaces," *arXiv preprint arXiv:2006.02201*, 2020.
- [26] H. Han, J. Zhao, Z. Xiong, D. Niyato, M. Di Renzo, Q.-V. Pham, and W. Lu, "Intelligent reconfigurable surface aided power control for physical-layer broadcasting," *arXiv preprint arXiv:1912.03468*, 2019.
- [27] S. Zhou, W. Xu, K. Wang, M. Di Renzo, and M.-S. Alouini, "Spectral and energy efficiency of IRS-assisted MISO communication with hardware impairments," *IEEE Wireless Commun. Lett.*, Early Access. 2020.
- [28] B. Ning, W. Hao, A. Zhang, J. Zhang, and G. Gui, "Energy efficiency–delay tradeoff for a cooperative NOMA system," *IEEE Wireless Commun. Lett.*, vol. 23, no. 4, pp. 732–735, Feb. 2019.

- [29] S. Sun, T. S. Rappaport, R. W. Heath, A. Nix, and S. Rangan, "MIMO for millimeter-wave wireless communications: Beamforming, spatial multiplexing, or both?" *IEEE Commun. Mag.*, vol. 52, no. 12, pp. 110–121, Dec. 2014.
- [30] M. R. Akdeniz, Y. Liu, M. K. Samimi, S. Sun, S. Rangan, T. S. Rappaport, and E. Erkip, "Millimeter wave channel modeling and cellular capacity evaluation," *IEEE J. Sel. Areas Commun.*, vol. 32, no. 6, pp. 1164–1179, Jun 2014.
- [31] O. El Ayach, S. Rajagopal, S. Abu-Surra, Z. Pi, and R. W. Heath, "Spatially sparse precoding in millimeter wave mimo systems," *IEEE trans. wireless commun.*, vol. 13, no. 3, pp. 1499–1513, Mar. 2014.
- [32] Y. Saito, Y. Kishiyama, A. Benjebbour, T. Nakamura, A. Li, and K. Higuchi, "Non-orthogonal multiple access (NOMA) for cellular future radio access," in *2013 IEEE 77th Veh Technol. Conf. (VTC Spring), Dresden, Germany*. IEEE, Dec, 2013, pp. 1–5.
- [33] Z. Ding, X. Lei, G. K. Karagiannidis, R. Schober, J. Yuan, and V. K. Bhargava, "A survey on non-orthogonal multiple access for 5G networks: Research challenges and future trends," *IEEE J. Sel. Areas Commun.*, vol. 35, no. 10, pp. 2181–2195, Oct. 2017.
- [34] L. Zhu, J. Zhang, Z. Xiao, X. Cao, D. O. Wu, and X.-G. Xia, "Joint tx-rx beamforming and power allocation for 5G millimeter-wave non-orthogonal multiple access networks," *IEEE Trans. Commun.*, vol. 67, no. 7, pp. 5114–5125, Mar. 2019.
- [35] S. Boyd and L. Vandenberghe, *Convex Optimization*. Cambridge university press, 2004.
- [36] P.-A. Absil, R. Mahony, and R. Sepulchre, *Optimization algorithms on matrix manifolds*. Princeton University Press, 2009.
- [37] G. C. Bento, O. P. Ferreira, and J. G. Melo, "Iteration-complexity of gradient, subgradient and proximal point methods on riemannian manifolds," *Journal of Optimization Theory and Applications*, vol. 173, no. 2, pp. 548–562, Mar. 2017.
- [38] Z. Yang, M. Chen, W. Saad, W. Xu, M. Shikh-Bahaei, H. V. Poor, and S. Cui, "Energy-efficient wireless communications with distributed reconfigurable intelligent surfaces," *arXiv preprint arXiv:2005.00269*, 2020.
- [39] S. Ali, E. Hossain, and D. I. Kim, "Non-orthogonal multiple access (NOMA) for downlink multiuser mimo systems: User clustering, beamforming, and power allocation," *IEEE access*, vol. 5, pp. 565–577, Dec. 2016.
- [40] Y. Li, M. Jiang, Q. Zhang, and J. Qin, "Joint beamforming design in multi-cluster miso noma intelligent reflecting surface-aided downlink communication networks," *arXiv preprint arXiv:1909.06972*, 2019.
- [41] B. R. Marks and G. P. Wright, "A general inner approximation algorithm for nonconvex mathematical programs," *Operations research*, vol. 26, no. 4, pp. 681–683, Jun. 1978.